International Journal of Environmental, Social and Economic Sustainability
www.ijeses.org

H. Benbouhenni et al., Vol. 1, No. 1, Month, 2026 | Research Article

Fractional-Order Error PID Control Based on Genetic Algorithm for Power Quality Enhancement in DFIG Wind Turbines

Habib Benbouhenni *‡, Fayssal Amrane**, Nicu Bizon***

* Department of Electrical Engineering, Faculty of Technology, Hassiba Benbouali University of Chlef, B.P 78C Ouled Fares, Chlef 02180, Algeria

** LAS Research Laboratory, Department of Electrical Engineering, Setif-1 University Ferhat ABBAS, 19000 Setif, Algeria

*** The National University of Science and Technology POLITEHNICA Bucharest, Pitești University Centre, 110040 Pitesti, Romania

(h.benbouhenni@univ-chlef.dz, amrane_fayssal@univ-setif.dz, nicu.bizon1402@upb.ro)

‡Corresponding Author: Habib Benbouhenni, Hassiba Benbouali University of Chlef, h.benbouhenni@univ-chlef.dz

Received: 19.02.2026 Accepted:17.03.2026

Abstract-To enhance power quality in multi-rotor power systems, this study proposes a novel intelligent control algorithm based on a fractional-order error-based proportional-integral-derivative (FOE-PID) regulator. A genetic algorithm was used to calculate the controller gains. A direct power control technique with pulse width modulation (DPC-PWM), regulated by FOE-PID controllers for dynamic regulation of active and reactive power, harmonic suppression, and voltage stabilization, is used to overcome the drawbacks of conventional controllers, such as the proportional-integral (PI) controller. Extensive MATLAB-based simulations conducted under variable wind speed show that the FOE-PID approach performs better than the PI controller in the following important performance metrics: response time, steady-state error, reactive power compensation, total harmonic distortion, and power ripple. Also, the robustness of the designed approach compared to other strategies is studied in terms of sensitivity to parameter changes (factory parameter changes of ±100% for resistors and -100% for coils) and sudden changes in wind speed. For smart and sustainable energy systems of the future, this makes it an extremely efficient control solution.

Keywords: Fractional-order error, doubly-fed induction generator, genetic algorithm, multi-rotor wind turbine, total harmonic distortion, direct power control, multi-rotor power systems.

1. Introduction

Wind power (WP) has grown rapidly, with global capacity reaching 1,174 GW by 2024, including 121 GW added in 2024. Onshore wind dominates (92.9% of total capacity in 2022), while offshore wind is expanding fast, projected to supply 34% of WP by 2050 [1]. China led installations in 2024 (87 GW, 72% of new capacity), and offshore wind set records in 2021 (17.4 GW globally). Costs have plummeted, with onshore LCOE (Levelized Cost of

Cite this article as: H. Benbouhenni, F. Amrane, and N. Bizon, "Fractional-Order Error PID Control Based on Genetic Algorithm for Power Quality Enhancement in DFIG Wind Turbines", International Journal of Environmental, Social and Economic Sustainability, (IJESES), Vol.1, No. 1, pp. 36-64, March, 2026.

Electricity) falling to $0.0331/kWh (2021). Europe added 14.7 GW in 2020, driven by offshore projects. By 2050, wind could provide 30% of global electricity, up from 10% today [2].

Figure 1 illustrates the evolution of offshore installation from 2010 to 2025. Figure 2 illustrates the evolution of onshore cumulative WP capacity (Giga Watts) from 2001 to 2025.

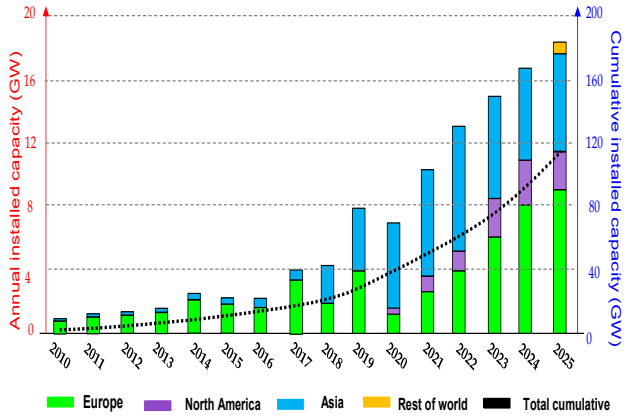

Fig. 1. Offshore installation from 2010 to 2025.

Wind turbines (WTs) convert kinetic energy from wind into electricity using various generator types, each suited to specific applications. The most common are horizontal-axis WTs (HAWTs), which dominate utility-scale projects due to their high efficiency (2–8 MW capacity) and ability to align perpendicular to wind direction via yaw systems [3]. These typically employ synchronous generators (e.g., permanent magnet or electrically excited) or asynchronous generators (e.g., squirrel cage or wound rotor). Synchronous generators offer precise grid synchronization but require full-power converters, increasing cost. In contrast, asynchronous generators are simpler and cheaper but lack variable-speed capability, reducing energy capture in fluctuating winds [4].

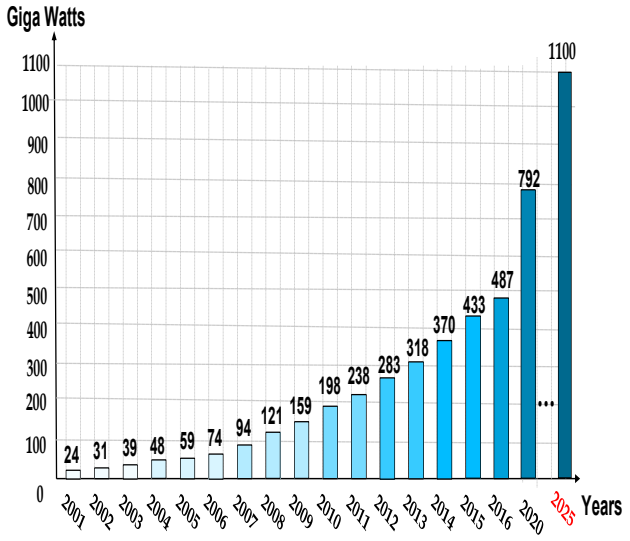

Fig. 2. Onshore cumulative WP capacity (Giga Watts) from 2001 to 2025.

Vertical-axis WTs (VAWTs), though less efficient, are used in urban settings due to omnidirectional operation and lower noise, often paired with direct-drive generators.

The doubly-fed induction generator (DFIG) stands out for its variable-speed operation and cost-effectiveness [5]. Unlike conventional generators, the DFIG's rotor is connected to the grid via a partial-scale converter (processing only 25–30% of total power), reducing converter costs and losses. This allows ±30% speed variation around synchronous speed, optimizing energy capture across wind conditions [6]. DFIGs also enable independent control of active and reactive power (Ps and Qs), enhancing grid stability by providing voltage support and fault-ride-through (FRT) capabilities during grid disturbances [7]. For instance, during voltage dips, DFIGs can inject reactive current to stabilize the grid, a feature absent in fixed-speed induction generators.

Compared to full-converter systems (e.g., permanent magnet synchronous generators), DFIGs reduce mechanical stress on WTs by allowing smoother torque adjustments, extending component lifespan [8]. They also outperform squirrel-cage induction generators in energy yield, as the latter dissipate slip power as heat, while DFIGs recirculate it via the rotor converter. Additionally, DFIGs are scalable for both onshore and offshore applications, with modern designs reaching 5 MW capacities [9]. Their lower maintenance needs (vs. gearless designs) and compatibility with existing grid infrastructure further solidify their dominance in wind farms. However, DFIGs require slip rings for rotor connections, introducing wear, and are sensitive to grid faults without protective crowbar circuits [10]. Despite these limitations, their balance of performance, cost, and grid support makes DFIGs the preferred choice for most large-scale WP projects [11].

Traditional vector control using PI controllers and pulse width modulation (PWM) in back-to-back converters faces several limitations, including high power ripples, slow dynamic response, and sensitivity to parameter variations [12]. The proportional integral (PI) controllers, though simple, struggle with nonlinearities and transient conditions, leading to poor disturbance rejection and steady-state errors (SSEs) in grid-tied applications [13]. PWM-based switching introduces total harmonic distortions (THDs) and electromagnetic interference, degrading power quality and increasing losses [14]. Additionally, the fixed-gain PI controllers lack adaptability to varying operating conditions, such as wind speed (WS) fluctuations in WP systems, resulting in suboptimal performance during rapid torque or power changes. The dual-loop control structure (outer voltage/inner current) further complicates tuning, often causing instability when grid impedance varies [15]. In back-to-back converters, the machine-side converter (MSC) and grid-side converter (GSC) require decoupled command of active/reactive power, but PI-based schemes exhibit cross-coupling issues, especially during low-voltage ride-through (LVRT) events [16].

For synchronous mode (rotor speed = synchronous speed), the generator operates at unity slip, ensuring stable power delivery but lacks flexibility for variable-speed applications like WTs. Super-synchronous mode (rotor speed > synchronous speed) enables higher energy extraction in WT systems but demands precise control to manage overvoltage and mechanical stress on the drivetrain [17]. Conversely, sub-synchronous mode (rotor speed < synchronous speed) is common during low-wind conditions but risks stator overcurrents and reactive power deficits, necessitating advanced control to maintain grid synchronization [18]. Modern solutions like adaptive PI controllers [19], model predictive control (MPC) [20], or synergetic control [21] are being explored to mitigate these drawbacks, offering better dynamic response and robustness. However, these methods increase computational complexity, highlighting the trade-off between performance and implementation feasibility in industrial systems.

Recent advancements in control systems for DFIG-based WP systems have significantly enhanced performance, robustness, and grid compliance. Backstepping control (BC) improves transient response by recursively stabilizing subsystems, ensuring Lyapunov stability, and handling nonlinearities like WS variations [22]. High-order sliding mode control (HOSMC), particularly super-twisting algorithms (STAs), reduces chattering while maintaining robustness against parameter uncertainties and grid faults, as validated in real WS profiles [23]. Prescribed sliding mode control (PSMC) combines adaptive gains with predefined convergence rates, optimizing power tracking and FRT capability [24]. H-infinity (H∞) control minimizes disturbances in grid voltage and mechanical torque fluctuations, ensuring stability under unbalanced grid conditions [25]. In the field of control, there are many new strategies that have been proposed as a solution to replace traditional strategies and overcome the most prominent challenges. The most prominent of these strategies that have recently emerged is the Event-triggered fuzzy reinforcement learning method, which was proposed in [26] to achieve optimal control of nonlinear systems of fractional order. This new strategy is based on deriving the fractional Hamiltonian-Jacobi-Bellman (HJB) equation by constructing an auxiliary system of equivalent integer order, and the fractional optimal solution is derived with an overall performance index. Two fuzzy logic (FL) systems are also used to form an actor-critic structure to approximate the cost function and the optimal controller, respectively. The stability of this strategy was verified using the Lyapunov function. This new strategy relies on the use of an event-triggered mechanism to reduce computational burden and avoid Zeno behavior. The effectiveness and efficiency of this approach were verified using the MATLAB environment. The results demonstrated the effectiveness and efficiency of this new approach, making it a viable solution for improving power quality in the field of renewable energy. In [27], the fractional HJB equation based on the error derivative is proposed to obtain an optimal equation for the fractional-order optimal control solution. This solution is proposed to avoid the failure of achieving asymptotically stable system. Actor-criticneural neural networks (NNs) were created to implement the boosting algorithm. The effectiveness of this approach was evaluated for improving the performance of an electromechanical converter system with a chaotic magnetic field. All results indicate the effectiveness of this strategy in improving the properties and advantages of the studied system. One of the major drawbacks of this approach is its complexity, making it a difficult solution to implement in the field of renewable energy. In [28], a practical reinforcement learning scheme for partially unknown fractional order nonlinear systems (FONS) is proposed using the fractional HJB equation. This equation contains the dynamics of FONS systems, by constructing an auxiliary system and an equivalent transformation. To approximate unknown dynamics functions and obtain approximate optimal regulators, RL, BC technique, and identifier-actor-critic NN techniques are used. Using these strategies makes this approach more complex. However, despite this complexity, this approach boasts high performance. This approach was validated using two different examples, and the results demonstrated how this designed approach can significantly improve efficiency and performance. Among the applications that addressed fractional control is work [29], which provided profound insights into the effect of fear, the dynamics of fractional-order control, and the effects of climate change on predator-prey interactions. The system's status is examined by analyzing the presence, uniqueness, limitations, and optimization of its solutions. Overall, this work provides a model for the application of fractional control in various fields, making it a reliable solution. In [30], a partial derivative of the Caputo type was used to study a partial ecological epidemiological model, which includes the effects of fear, treatment, and cooperation in hunting, to explore the effect of memory in the ecosystem. Numerical simulations were conducted for different values of the memory parameter and some model parameters to determine the effectiveness of using a partial derivative of the Caputo type. All numerical results show that the studied system exhibits stable behavior of a periodic or chaotic nature with increasing memory effect. The effects of climate change are represented by an exponential decay function. Fractional calculus can be used for biological studies, where the use of this strategy greatly contributes to understanding biological behavior. In the work [31], fractional calculus was used to study the dynamic behavior of an epidemic model to investigate two functions of the fear effect. In this work, the Caputo factor is used to develop a fractional-order epidemic model to study the impact of fear on pathogen environments and vaccination measures. This study demonstrates that fractal model solutions exist, are effective, and are unique, as confirmed by numerical simulations. In [32], the use of fractional-order derivatives to explain temporal dependencies and memory in ecological processes was studied. Fractional-order derivatives were relied upon to study the complex dynamics of predator-prey systems, taking into account the effects of fear stress, global warming, hunting cooperation, and memory effects on species interactions. This work aims to provide a more comprehensive understanding of the fundamental mechanisms governing the stability and

behavior of ecosystems using the fractional-order derivative model. The existence, equilibria, and stability of the system were studied mathematically using global stability analysis and Hopf bifurcation. Numerical simulations were performed to validate the analytical results, and the results demonstrated the ability of fractional-order derivatives to improve the stability and equilibrium of the system. The author sees in [33] that global warming has become a major concern for the environment, as it causes serious, and often unexpected, effects on species, affecting their abundance, genetic composition, behavior, and survival. Accordingly, it was proposed to study the effects of global warming on predator-prey dynamics using the Caputo fractional derivative strategy. The author suggests that the density of prey and predator species decreases as a result of increased global warming. However, global warming increases the abundance of prey and predator species. All possible equilibrium states for the system were identified and implemented in MATLAB. Numerical simulation results demonstrate the effects of fear, fractional calculus, and global warming on the model's behavior. The results also demonstrate the extent to which global warming affects predator species, which may destabilize the system, but it may eventually stabilize. Furthermore, the numerical results indicate that the fractional order model is more stable than the integer order model. In [34], fractional-order control is used to optimize the performance of a grid-tied green power system. This nonlinear controller has its gains adjusted using Golden Eagle Optimization. Using this algorithm increases the performance and efficiency of the fractional controller in improving the quality of the power output from the system. An application of fractional controllers was implemented in [35] to improve the performance of turbine systems. A two-degree-of-freedom (2-DOF) fractional-order-proportional-integral derivative (2-DOF-FOPID) controller is the proposed solution for controlling the frequency of the system under study. The gains of this proposed controller were adjusted using the Cuckoo search algorithm. The performance of the proposed 2-DOF-FOPID controller is compared with that of well-known tradtional regulators. MATLAB simulations show that, compared to widely used conventional PI and PID controllers, the designed 2-DOF-FOPID regulator exhibits superior response in terms of shorter transition time, lower overshoot, and wide robustness to limit frequency deviation within an acceptable range, considering the integral squared error as the objective function. These results make this approach of interest in other industrial applications such as electric vehicles and renewable energy water pumping systems.

MPC leverages real-time optimization to manage active/reactive power decoupling, achieving faster dynamics than PI-based methods, with reduced harmonic distortion [36]. MRAS (Model Reference Adaptive Systems) sensorless techniques estimate rotor position/speed by comparing stator current models, eliminating encoders and reducing maintenance [37]. MRAC (Model Reference Adaptive Control) adapts to parameter variations (e.g., rotor resistance) for consistent maximum power point tracking (MPPT) performance [38]. Fractional-order PI/proportional derivative (PD) (FOPI/FOPD) controllers enhance damping and frequency response by incorporating non-integer calculus [39], improving LVRT performance.

Active Disturbance Rejection Control (ADRC) compensates for unmodeled dynamics (e.g., grid faults) via extended state observers (ESOs), outperforming traditional proportional-integral derivative (PID) in transient scenarios [40]. Intelligent controllers like NN techniques [41] and neuro-FL systems learn nonlinear mappings for optimal torque/power regulation [42], adapting to changing wind conditions. Type-2 FL handles uncertainties in WS and grid impedance better than Type-1 [43], while Type-3 FL further refines rule-based adaptation for extreme volatility [44].

Recent advancements in optimization algorithms have significantly enhanced the power control of DFIG-based WTs, addressing challenges like grid instability, THDs, and transient response. Genetic algorithms (GAs) optimize PI controller gains in MSCs, reducing active power ripples by 71.42% and Qs overshoot by 92.85% compared to conventional methods [45]. The Salp Swarm Algorithm (SSA) improves LVRT capability by dynamically tuning crowbar resistance and DC-link capacitance, decreasing active power overshoot from 10.12×10^6 to 3.78×10^6 during faults [46]. For multi-objective optimization, an improved NSGA-II algorithm balances transient response and steady-state stability, outperforming traditional methods in harmonic suppression and mechanical wear reduction [47].

Machine Learning-based controllers are increasingly adopted. NN algorithms replace PI controllers in direct vector control (DVC), achieving a stator current THD of 0.13% and minimizing power ripples in dual-rotor systems [48]. FL control (FLC) cascaded with direct power control (DPC) reduces THD by 47.22% and improves dynamic response by 91.42% under variable WSs [49]. Adaptive neuro-fuzzy inference systems (ANFIS) hybridize with fractional-order controllers to handle parameter uncertainties, enhancing robustness in grid-fault scenarios [50].

Sliding mode control (SMC) variants, such as STA, eliminate chattering effects while maintaining robustness [51]. STA-based DPC method reduces power fluctuations by 30% and improves transient response under real wind profiles [52]. Prescribed SMC ensures predefined convergence rates for active/reactive power tracking, critical for LVRT compliance. MPC leverages real-time optimization to decouple power loops, achieving faster dynamics than PI-based methods and reducing THD [53].

Multilevel converters (MLCs) and modular multilevel converters (MMCs) significantly reduce THD compared to traditional two-level inverters [54]. Cascaded H-bridge (CHB) MLCs achieve THD <1.87% in grid-tied PV systems, outperforming two-level inverters (5.82% THD) 116 [55]. Neutral diode-clamped (NPC) converters reduce voltage stress and harmonics, with THD <3% in medium-voltage drives [56]. MMCs in HVDC applications leverage advanced modulation (e.g., SHE-PWM) to achieve THD <2%, while PSO-optimized iSHE-PWM further reduces THD by 30%

without additional submodules [57]. Flying capacitor topologies offer redundancy but require complex balancing, achieving THD <2.5% in industrial drives [58].

Metaheuristic algorithms like particle swarm optimization (PSO) [59] and Whale Optimization Algorithm (WOA) fine-tune controller parameters [60]. PSO-optimized DPC minimizes torque ripples by 37.5%, while WOA enhances PMSG-DFIG hybrid systems' fault tolerance [61]. Fractional-order PID (FOPID) controllers, tuned via the Gray Wolf Optimizer (GWO), improve damping and LVRT performance by incorporating non-integer calculus [62]. Simulation results show that the GWO-based FOPID controller offers satisfactory operational performance compared to conventional controllers. However, despite this performance, the problem of current and power ripples remains. Furthermore, in robustness testing, it was observed that this regulator was significantly affected by changes in system parameters, which necessitated the search for a more effective and robust regulator while maintaining the simplicity and ease of implementation that characterize the FOPID regulator.

Hybrid approaches combine these techniques. For example, STA + synergetic control reduces torque ripples in dual-rotor WTs [63], while GA-enhanced PI regulators validated via dSPACE 1104 hardware show superior Processor-in-the-loop test results. Future directions include digital twin-assisted optimization and artificial intelligence-augmented MPC for adaptive grid support [64]. By surveying the literature, the advantages of FOPID controllers for DFIG-WTs can be summarized as follows:

- **Enhanced flexibility and precision:** FOPID controllers generalize traditional PID controllers by introducing fractional-order integrals (λ) and derivatives (μ), providing two additional tuning parameters. This allows finer control over dynamic responses, improving precision in tracking active/reactive power references under variable wind speeds.
- **Superior robustness to parameter variations:** Unlike conventional PI/PID controllers, FOPID controllers maintain stability even when DFIG parameters (e.g., rotor resistance, inductance) deviate from nominal values, ensuring consistent performance despite machine aging or operating condition changes.
- **Improved transient response:** FOPID controllers reduce overshoot and settling time during power fluctuations. For example, studies show a 30–50% reduction in settling time for DC-link voltage regulation compared to integer-order PIs, critical for grid FRT scenarios.
- **Better harmonic suppression:** The fractional-order dynamics of FOPID controllers mitigate THD in stator currents. Experimental results demonstrate >50% THD reduction in grid currents when applied to MSCs.
- **Adaptability to nonlinearities:** WTs exhibit nonlinear aerodynamics and mechanical stress. FOPID controllers, tuned via Metaheuristics (e.g., Manta Ray Foraging Optimization, Walrus Algorithm), adapt to these nonlinearities, optimizing power extraction across sub/super-synchronous modes.
- **Reduced mechanical stress:** By minimizing torque ripples (up to 46% reduction), FOPID controllers extend the lifespan of drive train components, addressing a key challenge in two-mass WT systems.
- **Optimal MPPT performance:** FOPID controllers outperform traditional PIs in MPPT, achieving >95% efficiency in energy capture under turbulent wind profiles due to their adaptive fractional calculus-based tuning.
- **Grid stability support:** FOPID-enhanced DFIGs provide superior reactive power control during voltage dips, complying with grid codes (e.g., LVRT requirements) by dynamically adjusting λ and μ to stabilize grid voltage.
- **Computational efficiency with metaheuristics:** Modern algorithms like Ant Lion Optimization (ALO) and PSO efficiently tune FOPID parameters, reducing computational burden while maintaining robustness.
- **Future-readiness for hybrid systems:** FOPID controllers seamlessly integrate with artificial intelligence-based techniques (e.g., neuro-FL systems) and MPC, offering a pathway for next-generation adaptive WP systems.

Table 1 presents a comparative analysis of the proposed advanced control algorithms for DFIG power control. This table highlights the challenges hindering the deployment of the control strategies and their degree of robustness. It also highlights some of the key advantages of the proposed control strategies.

From the above studies, no control strategy has been found that can significantly reduce ripples while maintaining simplicity and ease of realization. Therefore, a fractional-order error-based PID (FOE-PID) controller is a suitable controller, being applied for the first time in multi-rotor WT DFIG systems. In this work, a FOE-PID regulator is designed to enhance the advantages and efficacy of DPC in DFIG systems. A GA is used to estimate the gain values of the FOE-PID regulator. Therefore, this work focuses on power control to ensure significant improvements in power quality. There are several simple, reliable solutions for enhancing the robustness and operational performance of DFIG-based multi-rotor WT systems. These simple, yet effective solutions can enhance the active and reactive power quality of these power systems. Furthermore, these simple solutions can reduce the THD of the current while maintaining the simplicity and ease of implementation of PI-type controls. These simple solutions are unexplored in the field of renewable energy, requiring extensive research to explore and implement them. They do not require complex equipment or significant costs.

Simulations can be used to explore the effectiveness of these simple solutions. Moreover, changing the parameters of the system under study requires the development of control algorithms that have significant potential to overcome this problem. Developing simple control strategies allows for improved stability of problems.

There is potential to leverage GAs to adjust the gains of properly designed regulators. There is a need to expand the application of GA technique-based FOE-PID (FOE-PID-GA) controllers with greater flexibility in controlling multi-rotor WT systems based on DFIG.

Multi-rotor WT systems based on DFIG are among the most prominent modern systems that have recently emerged as a suitable solution to overcome the problems of conventional systems. Therefore, it is necessary to consider ensuring the efficient, effective, and stable operation of these systems. This approach is an important field that poses theoretical issues and practical importance, with several challenges, most notably durability, power quality, stability, etc. To overcome the major challenges hindering the deployment of energy systems, particularly multi-rotor WT systems, a modern control strategy with significant potential to address these challenges must be proposed. The fractional-order error technique and the PI controller are among the most popular control strategies in the literature. Furthermore, the GA technique has been widely used in control to achieve optimal results and high accuracy.

Table 1. Comparative analysis of advanced control algorithms for DFIG power control

Control Method	Overshoot	Dynamic Response	THD (%)	Static Error	Complexity	Robustness	Ripple Ratio	Key Strengths	Limitations
Backstepping control [65]	Low (<5%)	Fast (0.1–0.3s)	1.8–3.5	Negligible	High (nonlinear Lyapunov design)	High (handlesparametricuncertainties)	20–30% reduction	Stability-guaranteed, adaptive to wind fluctuations	Computationally intensive
HOSMC technique [66]	Very Low (<2%)	Very Fast (<0.1 s)	1.5–2.5	Zero (finite-time convergence)	Moderate (requires gain tuning)	Very High (immune to disturbances)	40–50% reduction	Chattering-free, fault-tolerant	Sensitive to actuator saturation
H∞ control [67]	Moderate (5–10%)	Medium (0.3–0.5s)	2.0–3.0	Small (optimized via weighting functions)	High (frequency-domainsynthesis)	High (optimized worst-case performance)	15–25% reduction	Robust to grid impedance variations	Conservative tuning
Predictive MPC [68]	Low (<3%)	Fast (0.2–0.4s)	1.0–2.0	Near-zero (model-based prediction)	Very High (real-time optimization)	Moderate (depends on model accuracy)	50–60% reduction	Decoupled power control, handles constraints	High computational load
NN control [69]	Variable (3–8%)	Adaptive (0.2–0.6s)	1.2–2.8	Small (training-dependent)	Very High (black-box design)	Moderate (data-driven)	30–40% reduction	Self-learning, MPPT integration	Requires extensive training data

Type-2 FL technique [70]	Low (<4%)	Medium (0.3–0.5s)	1.5 – 2.5	Negligible (rule-based adaptation)	Moderate (membership tuning)	High (handlesuncertainties)	25–35% reduction	No need for precise models	Rule explosion for high-dimension systems
Type-3 FL technique [71]	Very Low (<2%)	Fast (0.1–0.3s)	1.0 – 1.8	Near-zero (hierarchicalrules)	High (3D membership functions)	Very High (superior uncertainty handling)	40–50% reduction	Enhancedgranularity for volatility	Complex implementation
ADRC [40]	Low (<5%)	Fast (0.1–0.3s)	1.8 – 2.5	Near-zero (ESO-based disturbance rejection)	Moderate (observer tuning)	Very High (model-independent)	35–45% reduction	Decouples dynamics, plug-and-play	Requires bandwidth tuning
MRAC [72]	Moderate (5–10%)	Adaptive (0.4–0.8s)	2.0 – 3.5	Small (reference model tracking)	High (adaptive law design)	Moderate (depends on reference model)	20–30% reduction	Self-tuning for parameter drift	Slow convergence
MRAS [73]	Low (<4%)	Medium (0.3–0.6s)	1.5 – 2.5	Small (sensorless estimation)	Moderate (adaptive observer)	High (reduces hardware costs)	25–35% reduction	Eliminatesencoders, cost-effective	Sensitive to initial estimates
FOPI control [74]	Low (<3%)	Medium (0.2–0.4s)	1.2 – 2.0	Near-zero (λ/μ tuning)	Moderate (fractionalcalculus)	High (flexible dynamics)	40–50% reduction	Improved damping, LVRT support	Non-intuitive tuning

In the field of control, these three algorithms have been used in various research projects in various ways and in different settings. However, they remain unexplored in the field of multi-rotor WT systems. The important contributions of this article are as follows:

- A PID controller based on fractional calculus and GAs is developed and its performance in regulating active and reactive power in DFIG-based multi-rotor WT systems is evaluated.
- The efficiency of the GA-based FOE-PID regulator is determined under challenging conditions, including WS variations, effective power adjustments, and parameter uncertainty.
- The simulation results generated using the FOE-PID-GA will be compared with the PI-GA regulator to evaluate the system's performance. The results will also be compared with related works.

The following is a summary of the significant improvements this research can offer in the field of multi-rotor WT systems and their integration into the electricity grid:

- Improving the performance of DFIG-based multi-rotor WT systems under variable wind conditions;
- Significantly improving power and current quality;
- Overcoming the problems of the DPC.
- Reduces both SSE and DFIG power overshoot compared to the PI technique.
- Improves the quality of the generated currents, with a lower THD value compared to the PI-GA regulator.
- Significantly increases the robustness of the control system.

The manuscript is organized as follows: Section 2 outlines the design of the suggested FOE-PID-GA controller. Section 3 describes the designed power control technique used to control the DFIG power. Section 4 presents the results and initiates the discussion. Finally, Section 5 summarizes the entire paper.

2. Proposed FOE-PID-GA Controller

The controller suggested in this paper is based on the development of the PID controller. The PID controller is

adopted due to its simplicity and ease of realization. This designed controller relies on the use of both the GA technique and fractional calculus to increase performance. According to the work done in [75], the PID controller expression is written in the form of Equation (1).

$$y(t) = k_1.e(t) + k_2 \int e(t).dt + k_3 \frac{de(t)}{dt} \quad (1)$$

Where, $e(t)$ is the error or surface.

Equation (2) expresses the transfer function of the PID regulator.

$$F_{PI} = \frac{K_3 s^2 + K_1 s + K_2}{s} \quad (2)$$

Despite its rapid dynamic response and ease of application, the PID controller produces unsatisfactory results in the event of a system malfunction. In the field of command, several solutions have been designed to overcome the problems of the PID controller. The most prominent of these solutions were the use of NNs [66], FLC [77], GA method [78], GWO technique [79], fractional-order control [80], etc. In some cases, the use of nonlinear strategies such as BC and SMC was proposed to replace the use of PID controllers in control [81, 82]. Using these solutions yields satisfactory results compared to a PID controller. However, they increase complexity and difficulty in tuning. These proposed solutions make the PID controller experimentally expensive, which is undesirable.

In this section, the FOE strategy is used with a GA method as a suitable solution to overcome the problems of the PID controller. These strategies were chosen for their simplicity, ease of use, and high strength, especially with regard to the FOE strategy. A different FOE strategy was adopted than the one used in the literature. A simple FOE strategy method was used that does not rely on the mathematical model of the system or the PID regulator. A GA method was used to calculate the optimal gain values for the designed regulator. The designed approach is based on applying fractional calculus to the error signal, where $e^{\alpha}(t)$ instead of just $e(t)$ is used, which makes this designed regulator completely different from the FOPID regulator.

The regulator designed in this section can be illustrated in Figure 3. Figure 3 gives a clear picture of the concept of the designed regulator, where simplicity, ease of configuration, and ease of implementation are the most prominent features of this regulator. Moreover, the controller's reliance on both the GA approach and the FOE technique makes it more robust and performant compared to many existing regulators, such as PI regulators or hysteresis comparators. To implement the GA approach in MATLAB, we rely on gatool. Using gatool does not require writing complex programs or performing any complex calculations, making the GA strategy a suitable choice for this paper. In this new algorithm, the integral of time-weighted absolute error (ITAE) was used to estimate the optimal values for the suggested regulator parameters.

The use of ITAE was chosen to determine the optimal values for the designed regulator because of its ability to produce good results and is also considered one of the most prominent errors used in the embodiment of intelligent algorithms. Equation (2) is used to embody ITAE in MATLAB. On the other hand, the characteristics of the GA technique used in this study are listed in the supplementary file (Table S1). This file lists all the values and characteristics used in the GA to extract the best gain values.

$$ITAE = \int_0^{\infty} t \times |e(t)| \times dt \quad (2)$$

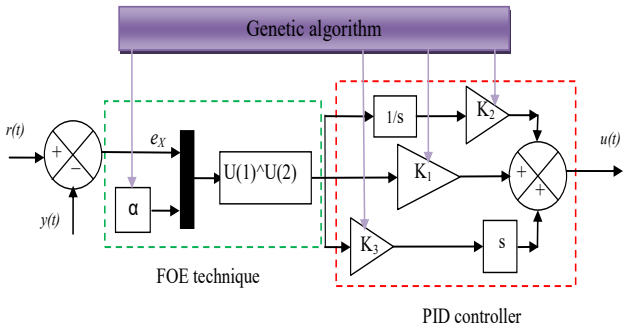

Fig. 3. Proposed PID-FOE regulator.

The controller parameters were optimized using a genetic algorithm. To ensure reproducibility, the main GA configuration parameters are briefly summarized here. The optimization process was performed with a population size of 20 individuals and a maximum of 100 generations. The stochastic uniform selection method was adopted, while the scattered crossover operator was used with a crossover fraction of 0.8. Mutation was applied using the default constraint-dependent mutation function to maintain population diversity. In addition, elitism was employed with an elite count of 2 to preserve the best individuals during the evolutionary process. The optimization involved four decision variables corresponding to the controller parameters, and the fitness evaluation was performed serially. The algorithm stopped when the maximum number of generations was reached or when the function tolerance criterion (10^{-6}) was satisfied. A detailed list of GA parameters is provided in Table S1 of the supplementary material.

According to Figure 3, the designed regulator can be modeled by Equation (3). Therefore, the modeling of the designed regulator is completely different from the modeling of the PID regulator included in Equation (1).

$$u(t) = k_1.e^{\alpha} + k_2 \int e^{\alpha}.dt + k_3 \frac{de^{\alpha}}{dt} \quad (3)$$

Where, e^{α} is the FOE and $u(t)$ is the output of the proposed regulator.

K_1, K_2, and K_3 are the designed regulator gain values.

The dynamic response of the designed regulator can be controlled and varied by using gain values.

So, in FOE-PID, the non-integer operator is applied to the error, rather than directly to the controller terms.

In this designed regulator, the α value must not be set to 0. If the value of alpha is equal to 1, then Equation (3) becomes Equation (1), where in this case the designed regulator

becomes a PID controller. Therefore, the shape of the designed regulator can be regulated by the value of α. In other words, the new regulator plays the role of two regulators at once, with the value of α being passed from one controller to the other. This feature is not found in conventional regulators in the literature, making this proposed regulator of great importance. This designed regulator is completely different from the regulators proposed in research works [83-85] in terms of structure, performance, efficiency, simplicity, ease of application, and dynamic response.

In Table 2, a comparison is made between the designed controller (FOE-PID-GA) and the FOPID controller to illustrate how the designed controller differs from this controller. Table 2 highlights the similarities between the two controllers, noting that the two controllers are completely different from each other in terms of structure and principle. In terms of the number of gains, the FOE-PID-GA regulator has less gain than the FOPID regulator, making it easier to adjust and thus easier to use in control. The designed regulator has less computational complexity than the FOPID regulator because only one fractional calculus is applied to the error, whereas in the FOPID regulator the fractional calculus is applied to both the integration and differentiation. Therefore, Table 2 highlights the extent of the contribution made in this paper, which makes this work of great importance in the field of control first and in the field of energy second.

Table 2. Comparison between FOPID and FOE-PID-GA regulators

Aspect	FOPID	FOE-PID-GA
Model	$y(t) = k_p + k_i s^{\alpha} + k_d s^{-\tau}$	$y(t) = K_2 \int e^{\alpha}.dt + K_1.e^{\alpha} + K_3 \frac{d\,e^{\alpha}}{dt}$
Number of gains	5	4
Fractional element	In controller: s^{α} and $s^{-\tau}$	On the error: $e^{\alpha}(t)$
Computational load	High (especially with two fractional orders)	Potentially lower if only one fractional operator on error
Implementation	Requires fractional derivative/integral operators in control loop	Requires fractional operator applied to error signal
Hardware feasibility	Moderate to high complexity	Simple
Approximation method	Oustaloup or similar	Likely Oustaloup as well

The stability of the regulator designed in this paper is studied using Lyapunov's theorem. Equation (3) is used to extract the stability conditions.

Error ($e(t)$) can be written as follows:

$$e(\mathrm{t}) = \mathrm{r}(\mathrm{t}) - \mathrm{y}(\mathrm{t}) \tag{4}$$

The designed controller is a nonlinear PID controller. The stability of this designed closed-loop controller is analyzed.

To apply the Lyapunov method, the entire closed-loop system, including the system itself, must be analyzed. Let's assume a simple second-order system for clarity:

$$\ddot{x} = u(\mathrm{t}) \tag{5}$$

Also, the state space can be written as represented in Equation (6).

$$\begin{cases} \dot{x}_2 = u(\mathrm{t}) \\ \dot{x}_1 = x_2 \end{cases} \tag{6}$$

Equation (4) can be written as follows:

$$e(\mathrm{t}) = x_1 - x_d(\mathrm{t}) \tag{7}$$

Then:

$$\dot{e}(\mathrm{t}) = \dot{x}_1 - \dot{x}_d(\mathrm{t}) = x_2 - \dot{x}_{\mathrm{d}} \tag{8}$$

The second derivative of Equation (8) is written as follows:

$$\ddot{e}(\mathrm{t}) = \dot{x}_2 - \ddot{x}_{\mathrm{d}} = u - \ddot{x}_{\mathrm{d}} \tag{9}$$

The control law is represented by Equation (10), by which the stability is proven.

$$u(\mathrm{t}) = \mathrm{k}_2 \int (\mathrm{e}^{\alpha})\mathrm{dt} + \mathrm{k}_1(\mathrm{e}^{\alpha}) + \mathrm{k}_3 \frac{\mathrm{d}}{\mathrm{dt}}(\mathrm{e}^{\alpha}) \tag{10}$$

To prove the stability, a Lyapunov function of the form ($V(e,\dot{e})$) is defined. The derivative of this function is then calculated. The stability condition is proven or extracted from the derivative of the Lyapunov function.

Equation (11) represents the Lyapunov function used in this work to prove the stability of the designed regulator.

$$V(e,\dot{e}) = \frac{1}{2}\dot{\mathrm{e}}^2 + \frac{\mathrm{k}_1}{\alpha+1}\mathrm{e}^{\alpha+1} \tag{11}$$

Where, $\frac{\mathrm{k}_1}{\alpha+1}\mathrm{e}^{\alpha+1}$ is the potential energy form nonlinear error term, ensures positivity if $\alpha + 1 > 0$.

$\frac{1}{2}\dot{\mathrm{e}}^2$ is the standard kinetic energy term.

The function in Equation (11) is positive definite if $e \neq 0$ and $e=0$.

The derivation of Equation (11) is written as follows:

$$\dot{V}(e,\dot{e}) = \dot{\mathrm{e}}.\mathrm{e} + (\alpha+1)\frac{\mathrm{k}_1}{\alpha+1}\dot{\mathrm{e}}.\mathrm{e}^{\alpha} \tag{12}$$

So,

$$\dot{V}(e,\dot{e}) = \ddot{\mathrm{e}}.\mathrm{e} + \mathrm{k}_1\dot{\mathrm{e}}.\mathrm{e}^{\alpha} \tag{13}$$

Based on Equations (9) and (10), Equation (14) can be written.

$$\ddot{e} = \mathrm{k}_2 \int (\mathrm{e}^{\alpha})\mathrm{dt} + \mathrm{k}_1(\mathrm{e}^{\alpha}) + \mathrm{k}_3 \frac{\mathrm{d}}{\mathrm{dt}}(\mathrm{e}^{\alpha}) - \ddot{x}_{\mathrm{d}} \tag{14}$$

The derivative of the Lyapunov function can be written as:

$$\dot{V}(e,\dot{e}) = \dot{e}(k_2 \int(e^{\alpha})dt + k_1(e^{\alpha}) + k_3 \frac{d}{dt}(e^{\alpha}) - \ddot{x}_d) + k_1 \dot{e}.e^{\alpha} \quad (15)$$

Equation (15) becomes as follows:

$$\dot{V}(e,\dot{e}) = \dot{e}(k_2 \int(e^{\alpha})dt + 2.k_1(e^{\alpha}) + k_3 \frac{d}{dt}(e^{\alpha}) - \ddot{x}_d) \quad (16)$$

Assume that $\ddot{x}_d$ equals 0 for step response tracking (setpoint is constant), and that $\alpha > 0$, Equation (16) becomes as follows:

$$\dot{V}(e,\dot{e}) = \dot{e}(k_2 \int(e^{\alpha})dt + 2.k_1(e^{\alpha}) + k_3 \alpha (e^{\alpha-1})) \quad (17)$$

With:

$$\frac{d}{dt}(e^{\alpha}) = \alpha e^{\alpha-1}\dot{e} \quad (18)$$

Based on Equation (17), Equation (19) can be written.

$$\dot{V}(e,\dot{e}) = \dot{e}(k_2 \int(e^{\alpha})dt + 2.k_1(e^{\alpha})) + k_3 \alpha (e^{\alpha-1})\dot{e}^2 \quad (19)$$

Some conditions are imposed to ensure that Equation (19) is negative.

The term $k_3(e^{\alpha-1})\alpha.\dot{e}^2$ is positive definit if $\alpha > 0$ and $e \neq 0$.

The term $\dot{e}(k_2 \int(e^{\alpha})dt + 2.k_1(e^{\alpha}))$ can have either sign depending on the condition of $\dot{e}$.

In the case of e=0 and $\dot{e} = 0$, local stability can be guaranteed. Therefore, the controller is considered to be locally asymptotically stable under the following conditions:

$$\begin{pmatrix} k_1, k_2, k_3 > 0 \\ \alpha > 0 \end{pmatrix} \quad (20)$$

The conditions listed in Equation (20) are satisfied, so the Lyapunov function is positively definite, and consequently the derivative of the Lyapunov function is negatively definite, and possibly negatively definite in some region. Therefore, the system is considered locally stable.

This designed regulator is used in this paper to command the power of a DFIG-MRWT. The competence and efficiency of this regulator in enhancing the output power quality and reducing the THD of current compared to a conventional PI regulator are investigated. The next section discusses the application of the designed regulator in DFIG power control, highlighting its advantages and disadvantages.

3. Proposed Power Control Technique

The approach suggested in this study is based on the use of a FOE-PID-GA controller, where one regulator is used for active power and another for reactive power. This approach aims to reduce power ripples and THD while maintaining simplicity and ease of realization. This proposed control approach is an improvement over the traditional DPC-PI approach, where a FOE-PID-GA controller is used instead of a PI controller. A FOE-PID-GA controller is used to determine voltage reference values. These values are calculated based on the power error.

Figure 4 represents the architecture of the power control approach for the DFIG-multi-rotor WT system. This figure shows that the approach applied in this study is completely different from several research works proposed in [86-88] in terms of principle, regulator used, simplicity, robustness, and fast dynamic response.

This algorithm is applied to the machine inverter only, as shown in Figure 4, to simplify the system and demonstrate its efficacy without the need to command the grid inverter or use filters. The control process begins by measuring the instantaneous active and reactive power of the system. These measured values P_{meas} and Q_{meas} are compared with their corresponding reference values P_{ref} and Q_{ref}.

The errors are calculated as follows: e_P=P_{ref}−P_{meas} and e_Q=Q_{ref}−Q_{meas}

These error signals represent the deviation between the desired and actual operating conditions of the system.

The active and reactive power errors are then processed by the FOE-PID controllers. The FOE-PID controller uses fractional calculus to provide additional tuning flexibility, allowing better control performance under varying load conditions. Each controller adjusts the control signals based on the magnitude and dynamics of the power errors.

The controller outputs generate intermediate control signals that correspond to the required adjustments in the inverter voltage components.

On the other hand, the designed approach relies on a PWM strategy to control the machine's inverter, making it inexpensive and easy to realize.

In this new algorithm, a two-level inverter is used to power the generator's rotor. Also, a non-controlled inverter is used to simulate the grid inverter.

In this designed approach, the reference value for the direct rotor voltage (V_{dr}^*) is determined based on the reactive power error (e_{Qs}).

In this designed strategy, the MPPT algorithm used to generate the *Ps* reference is specifically based on the Optimal Torque Control method, which determines the reference electromagnetic torque according to the optimal power-speed relationship of the wind turbine. The corresponding effective power reference is then obtained and regulated by a PI controller to ensure accurate tracking.

The reference value for the quadrature rotor voltage (V_{qr}^*) is determined by the active power error (e_{Ps}). The power error is determined according to Equation (21).

$$\begin{cases} e_{Ps} = P_s^* - P_s \\ e_{Qs} = Q_s^* - Q_s \end{cases} \quad (21)$$

Where, P_s^* is the reference value of active power and Q_s^* is the reference value of reactive power.

In the proposed control technique, the reference value of the direct rotor voltage is calculated based on Equation (3) and

Equation (21). This value is calculated according to Equation (22). This value is adjusted using the gains K_1 to K_3 and α. Equation (22) is embodied by Figure 5.

$$V_{dr}^{*} = k_1.e_{Q_s}^{\alpha} + k_2 \int e_{Q_s}^{\alpha}.dt + k_3 \frac{de_{Q_s}^{\alpha}}{dt} \quad (22)$$

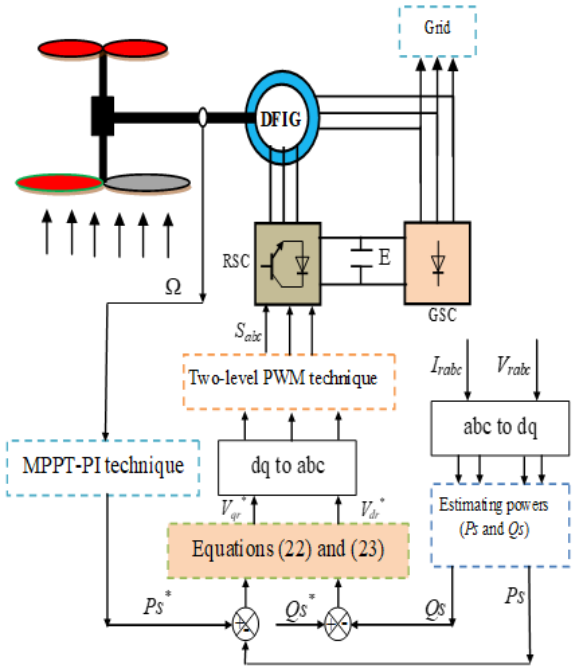

Fig. 4. Proposed power control of DFIG.

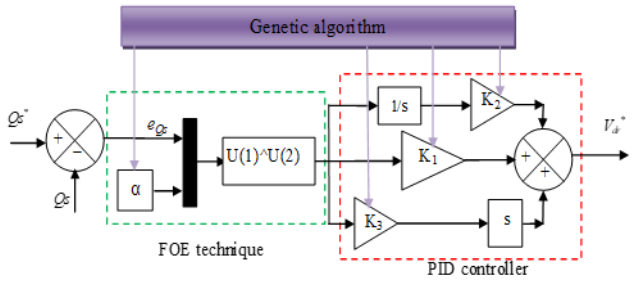

Fig. 5. Proposed reactive power regulator.

Using Equation (3) and Equation (21), the reference value of the quadrature voltage is estimated according to Equation (23). Figure 6 represents the mathematical model of the regulator included in Equation (23).

$$V_{qr}^{*} = k_1.e_{P_s}^{\alpha} + k_2 \int e_{P_s}^{\alpha}.dt + k_3 \frac{de_{P_s}^{\alpha}}{dt} \quad (22)$$

The gain values of these controls are calculated in this paper using a GA. The features of the GA used to estimate the optimal gain values for the active and reactive power regulator are listed in the supplementary file. On the other hand, the reference value of active power is determined in this paper using the MPPT-PI strategy. Using the MPPT-PI, the current, torque, and power are varied according to the WS profile.

To estimate the power error, the power must first be estimated. The power estimation in this new algorithm is the same as the power estimation used in the DPC. Power estimation in this new approach requires flux estimation. As is well known, flux estimation requires only current and voltage measurements.

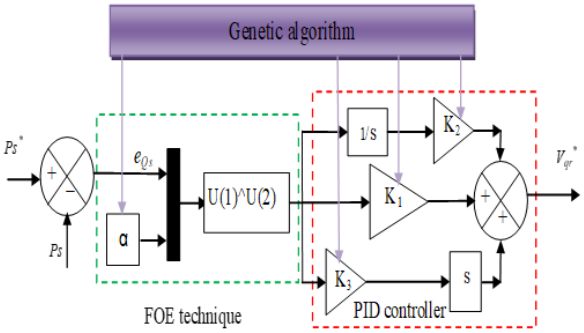

Fig. 6. Proposed active power regulator.

Based on the work performed in [89], the flux is estimated according to Equation (24).

$$\begin{cases} \Psi_{r\alpha} = \int_0^t (-R_r I_{r\alpha} + V_{r\alpha})dt \\ \Psi_{r\beta} = \int_0^t (-R_r I_{r\beta} + V_{r\beta})dt \end{cases} \quad (24)$$

Where, $V_{r\beta}$ and $V_{r\alpha}$ are the voltage linkage of β and α-axis.

$\Psi_{r\beta}$ and $\Psi_{r\alpha}$ are the flux linkage of β and α-axis.

Equation (25) can be used to estimate the rotor flux from the voltage.

$$|\bar{\Psi}_r| = \frac{|\bar{V}_r|}{w_r} \quad (25)$$

Where, V_r is the rotor voltage and Ψ_r is the rotor voltage.

Equation (24) can also be used to calculate the flux of the rotating part, while Equation (26) is used for this purpose.

$$\Psi_r = \sqrt{\Psi_{r\alpha}^2 + \Psi_{r\beta}^2} \quad (26)$$

According to the works [90, 91], the estimation of capabilities is estimated using Equations (27) and (28).

$$P_s = -\frac{3}{2}\frac{Lm.Vs.\psi_{r\beta}}{\sigma.Ls.Lr} \quad (27)$$

Where, Lm is the mutual inductance, R_s is the stator restiance, L_r is the rotor inductance, L_s is the stator inductance, and V_s is the stator voltage.

$$Q_s = -\frac{3}{2}\left(\frac{Vs}{\sigma.Ls} \cdot \psi_{r\beta} - \frac{Vs.Lm.\psi_{r\alpha}}{\sigma.Ls.Lr}\right) \quad (28)$$

With:

$$\sigma = 1 - \frac{M^2}{L_r L_s} \tag{29}$$

4. Results

The FOE-PID-GA strategy was validated using MATLAB 2014, comparing its efficiency with that of the PI-GA regulator and STA technique. The proposed regulator was implemented on a 1.5 MW generator. Four different tests were proposed for comparison. The efficiency was compared in terms of THD, overshoot, SSE, power ripples, response time, and strength. The parameters of the studied system are listed in Table 3.

Table 3. System parameters

Parameter		Values
Multi-rotor WT	Number of turbine blades	3
	r_1	1 m
	R_2	25.5 m
	Number of secondary WT blades	3
	J_2	1000 Kg.m^2
	r_g	0.75 m
	R_1	13.2 m
	r_2	0.5 m
	J_1	500 Kg.m^2
DFIG	P_{sn}	1500 kW
	p	2
	f_r	2.4 mN.m/s
	R_r	21 mΩ
	L_r	13.6 mH
	J	1 Mg.m^2
	fs	50 Hz
	L_s	13.7 mH
	L_m	13.5 mH
	Vs	380/696 V
	R_s	12 mΩ

A. First test: With the MPPT technique

The MPPT strategy is used to test the effectiveness of the new algorithm with varying WS profiles. Figure 7 and Table 4 represent the results of this test for three controls proposed in this paper. A zoomed-in graphical representation of these test results is included in Figure 8.

Figure 7a represents the WS used in this paper to study the effectiveness of the proposed control techniques in this study. Figure 7b shows the reactive power of the three algorithms. It is observed that this power closely follows the reference value, with ripples and a fast dynamic response for all three controls. Note that the reactive power does not change with WS, remaining constant at 0 VAR. According to Figure 8a, the reactive power ripples are lower when using the FOE-PID-GA controller than when using the PI-GA controller and the STA strategy. The values of these ripples are listed in Table 4. According to Table 4, the FOE-PID approach reduced the reactive power ripples by 90.48% and 65.59% compared to PI-GA and STA, respectively. Table 4 also shows that the FOE-PID-GA algorithm yielded better values for both SSE and ITAE of reactive power compared to the other strategies. In the case of ITAE, the FOE-PID-GA approach reduced this value by 64.03% and 22.58% compared to PI-GA and STA, respectively. In the case of SSE of reactive power, the FOE-PID-GA regulator reduced this value by 97.07% and 83.54% compared to PI-GA and STA, respectively. Despite this high performance, the FOE-PID-GA controller yielded unsatisfactory results for both response time and overshoot, as shown in Table 4. Therefore, the response time and overshoot values are considered the negatives of the FOE-PID-GA controller in this test. This negative can be attributed to the gain values.

Figure 7c shows the variation of active power for the three algorithms under the MPPT strategy. According to this figure, the active power for the three algorithms closely follows the reference value with a fast dynamic response. Also, it is noted that the active power varies with the change in WS, with the negative value for all three controls indicating that the system is in power generation mode. There are also ripples in this power level, as shown in Figure 8b and Table 4. These ripples are significantly lower when using the FOE-PID-GA regulator compared to other regulators. According to Table 4, active power ripples are reduced by 86.55% and 51.92% with the FOE-PID-GA regulator compared to the PI-GA and STA regulators, respectively. These ratios demonstrate the effectiveness of the designed regulator in improving active power quality. Furthermore, Table 4 shows that the FOE-PID-GA regulator yielded better values for SSE, overshoot, and ITAE than the other strategies. Thus, the FOE-PID-GA regulator reduced the active power ITAE, overshoot, and SSE by 67.47%, 19.81%, and 99.65%, respectively, compared to the PI-GA regulator. Furthermore, this design reduced the active power ITAE and SSE by 39.17% and 99.10%, respectively, compared to the STA regulator. However, the designed regulator gave unsatisfactory values for both overshoot and response time of active power compared to the other regulators, as listed in Table 4. The STA regulator gave a better value of overshoot of active power than the designed regulator by a percentage of 90.65% compared to the FOE-PID-GA regulator. Moreover, the response time of active power was better in the case of using both PI-GA and STA by percentages of 65.76% and 19.40%, respectively, compared to the FOE-PID-GA regulator.

Figure 7d represents the variation of torque over time for the three algorithms using MPPT. Note that the torque for three algorithms varies with the change in active power, with fluctuations. Also, note that the torque has negative values for three algorithms, proving that the system under study is sending power to the grid. According to Figure 8c, the torque ripples are significantly lower in the case of using the new algorithm compared to PI-GA and STA. The torque ripples in this test were estimated at 323.36 N·m, 109.80 N·m, and 30

N·m for the PI-GA, STA, and FOE-PID-GA, respectively. These values demonstrate that torque ripples are significantly reduced with the FOE-PID-GA, with a reduction of 90.72% compared to the PI-GA regulator and 72.67% compared to the STA technique.

Figure 7e represents the current variation for the three algorithms discussed in this article. According to Figure 7e, the current varies with the WS, with ripples present. The current also has a sinusoidal shape for both algorithms, as shown in Figure 8d. Furthermore, it is noted that the current signal has a period of 0.02 seconds in the case of the three controls. The current ripples in this test were estimated to be 120 A, 40 A, and 11.26 A for PI-GA, STA, and FOE-PID-GA, respectively. These values indicate that the FOE-PID-GA reduced current ripple by 90.61% and 71.85% compared to the PI-GA and STA, respectively. These figures demonstrate the FOE-PID-GA's significant effectiveness in improving current quality, making it a reliable solution for future control applications.

Figures 7f, 7g, and 7h represent the THD values for the three strategies. From these figures, the THD values were estimated to be 6.40% for PI-GA, 2.96% for STA, and 2.60% for FOE-PID-GA. These values indicate that the THD is significantly better for the FOE-PID-GA regulator compared to both PI-GA and STA, demonstrating its effectiveness and operational performance. Thus, the designed regulator reduced the THD by 59.37% and 12.16% compared to PI-GA and STA, respectively. Figures 7f, 7g, and 7h show that the fundamental signal amplitudes were 775.60 A, 779.30 A, and 770.20 A for PI-GA, STA, and FOE-PID-GA, respectively. From these values, it is evident that the FOE-PID-GA regulator yielded unsatisfactory amplitudes compared to the other regulators. Therefore, it can be concluded that the amplitude is also negative in this test. These shortcomings can be overcome in the future using other strategies, such as neural networks.

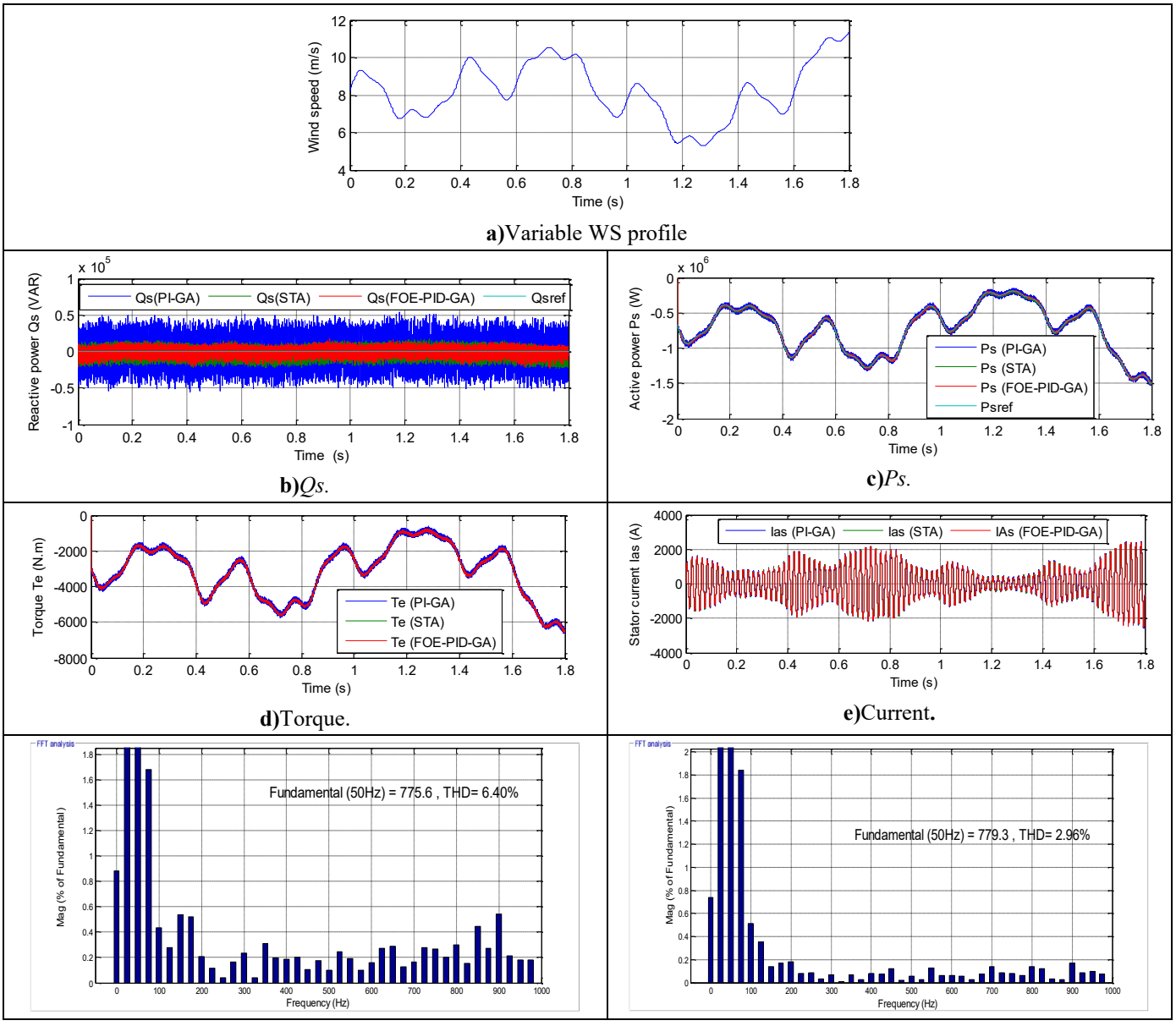

a)Variable WS profile

b)*Qs*.

c)*Ps*.

d)Torque.

e)Current.

f)THD(PI-GA).	**g)**THD(STA).

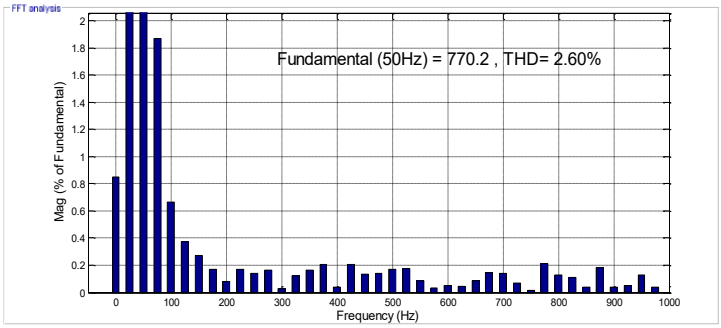

g)THD(FOE-PID-GA).

Fig. 7. First test results.

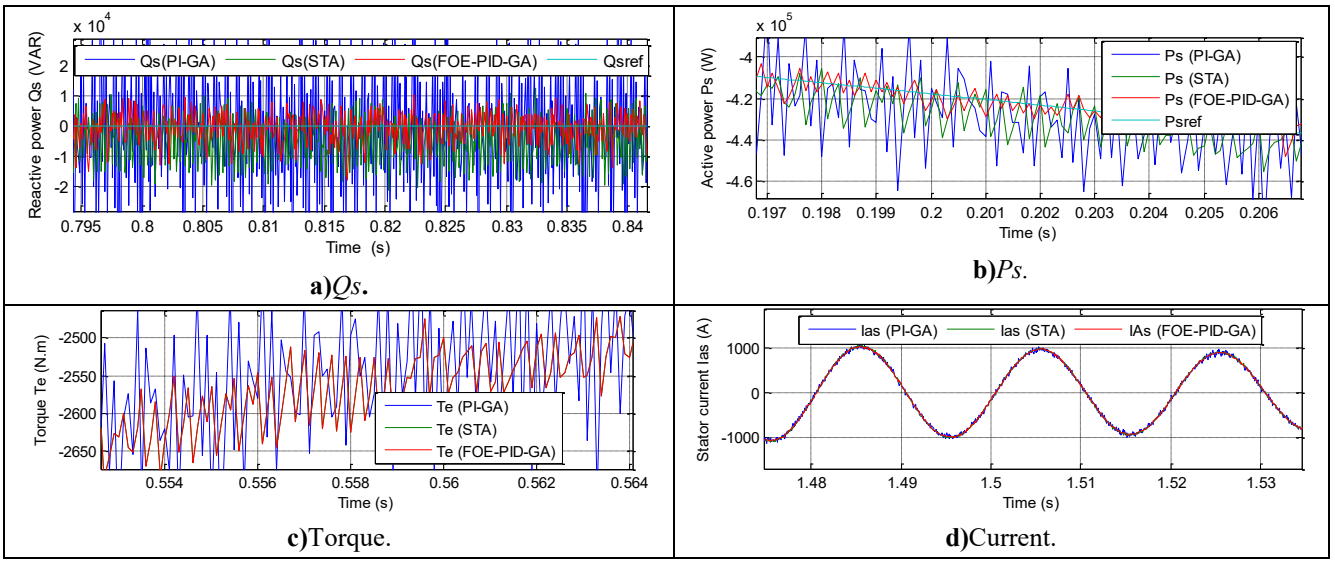

a)*Qs*. **b)***Ps*.

c)Torque. **d)**Current.

Fig. 8. First test results.

Table 4. Values and reduction ratios in the first test case.

Techniques		***Qs* (VAR)**	***Ps* (W)**
PI-GA	**Overshoot**	8219.40	22150
	Ripples	105106	90000
	Response time (ms)	0.069	1.27
	ITAE	17560	17720
	SSE	39085	29000
ST49 A	**Overshoot**	130.40	1660
	Ripples	29067	25170
	Response time (ms)	0.19	2.99
	ITAE	8159	9476
	SSE	6910	11200
FOE-PID-GA	**Overshoot**	10798	17760
	Ripples	10000	12100
	Response time (ms)	0.45	3.71
	ITAE	6316	5764
	SSE	1136.80	100

Ratios (%)	**Overshoot**	**FOE-PID-GA/PI-GA**	-23.88	19.81
		FOE-PID-GA/STA	-98.79	-90.65
	Ripples	**FOE-PID-GA/PI-GA**	90.48	86.55
		FOE-PID-GA/STA	65.59	51.92
	Response time (ms)	**FOE-PID-GA/PI-GA**	-84.66	-65.76

		FOE-PID-GA/STA	-57.77	-19.40
	ITAE	**FOE-PID-GA/PI-GA**	64.03	67.47
		FOE-PID-GA/STA	22.58	39.17
	SSE	**FOE-PID-GA/PI-GA**	97.09	99.65
		FOE-PID-GA/STA	83.54	99.10

As observed in Table 4, the proposed FOE-PID-GA controller exhibits a slightly longer response time compared with the PI-GA controller. This behavior is mainly related to the gain values obtained through the genetic algorithm optimization, which were tuned to prioritize steady-state performance, particularly ripple minimization and THD reduction. It is worth noting that alternative or hybrid optimization techniques, such as Particle Swarm Optimization (PSO) or hybrid GA–PSO methods, could potentially provide a more balanced tuning of the controller parameters. Such approaches may improve the transient response while maintaining the advantages of the FOE-PID structure in terms of harmonic mitigation and output waveform quality. This aspect will be considered as a potential direction for future work.

B. Second test

The strength of the new algorithm is investigated in this test under variable generator parameters, comparing its performance with the PI-GA and STA techniques. All inductances values are divided by 2, and all resistance values are multiplied by 2. The results obtained in this test are presented in Figures 9 and 10, while numerical results and reduction ratios are presented in Table 5.

Figure 9a represents the reactive power of three controls as the generator parameters change. This figure demonstrates that despite the parameter changes, the reactive power remains constant and closely follows the reference value for three control techniques, even with fluctuations. These ripples, as shown in Figure 10a, are significantly higher in the PI-GA and STA algorithms than in the FOE-PID-GA regulator. According to Table 5, the FOE-PID-GA regulator yielded better values for ITAE, ripples, SSE, and overshoot than the other strategies. Compared to the PI-GA regulator, FOE-PID-GA reduced ITAE, ripples, SSE, and overshoot by 65%, 80%, 96%, and 16.49%, respectively. The ITAE, ripples, SSE, and overshoot of the reactive power were reduced by 12.17%, 30.10%, 90.30%, and 7.55%, respectively, compared to the STA regulator. These ratios indicate the effectiveness of the designed approach despite the change in machine parameters and its significant ability to improve reactive power characteristics. However, in terms of reactive power response time, this regulator yielded unsatisfactory values compared to other strategies. Therefore, the reactive power response time in this test is also considered a disadvantage of the designed regulator.

Figure 9b represents the variation in active power for the three algorithms as the generator parameters change. This figure shows that despite changes in DFIG parameters, the active power continues to vary with changes in WS. It is noticeable that changes in generator parameters significantly affect this power, as this effect is evident in the higher ripples for the three controls compared to the first test. Furthermore, despite changing the DFIG parameters, the active power of the three controls remains negative, indicating that the system is in power generation mode. Figure 10b represents the amplified active power of the three controls. This figure demonstrates that the active power ripples are lower with the FOE-PID-GA regulator compared to the other strategies. The values of these ripples according to Table 5 ares better by percentages estimated at 87.88% and 54.49% compared to both PI-GA and STA, respectively. According to Table 5, the overshoot, ITAE, and SSE values are 95.12%, 59.95%, and 98.46% better than PI-GA, respectively. Compared to STA, the overshoot, ITAE, and SSE values are 90.36%, 20.16%, and 70.27% lower, respectively.

Figure 9c represents the torque change of the generator in the case of using the algorithms designed in this paper. From this figure, it's noticeable that the torque is significantly affected by variations in the DFIG parameters, as evidenced by the higher ripples compared to the first test. However, despite the changes in the generator parameters, the torque remains negative and varies according to the variation in active power. According to Figure 10c, the torque ripples were estimated to be 700 N·m, 200 N·m, and 80 N·m for PI-GA, STA, and FOE-PID-GA, respectively. With these values, torque ripples are 88.57% lower than with the PI-GA and 60% lower than with the STA.

Figure 9d represents the change in the current pattern when the DFIG parameters are varied for three control starategies. This figure shows that the current remains sinusoidal with ripples. The current value of the three controls in this test keeps changing as the wind speed changes. According to Figure 10d, the period of the current signal for both algorithms is 0.02 seconds. On the other hand, as shown in Figure 10d, the current ripples are significantly lower when using the FOE-PID-GA algorithm compared to the PI-GA and STA methods. These ripples are estimated to be 149.50 A, 65.10 A, and 33.30 A for PI-GA, STA, and FOE-PID-GA, respectively. Therefore, the current ripples are better with the FOE-PID-GA regulator, with ratios of 77.72% and 48.84% compared to the PI-GA and STA regulators, respectively. This ratio demonstrates the significant effectiveness of the FOE-PID-GA regulator in improving current quality despite varying generator parameters, making it a promising solution.

Figures 9e, 9f, and 9g represent the THD values for the algorithms designed in this study. These figures demonstrate that the THD value was significantly affected by changes in

machine parameters, with a significant increase in the THD value compared to the first test. According to these figures, the THD value for the PI-GA approach was estimated to be 12.71%, while for the FOE-PID-GA approach, the THD value was estimated to be 4.07%. In the STA approach, the current THD value was estimated to be 4.70%. These values demonstrate that the THD value is better with the FOE-PID-GA approach compared to the other strategies. This THD reduction is estimated to be 67.97% compared to the PI-GA approach and 13.40% compared to the STA approach. According to Figures 9e, 9f, and 9g, the fundamental signal (50 Hz) amplitude in this test was estimated to be 788.60 A, 787.70 A, and 781 A for PI-GA, STA, and FOE-PID-GA, respectively. The obtained values indicate that the PI-GA regulator gave better amplitudes than the FOE-PID-GA and STA regulators, with ratios of 0.96% and 0.1%, respectively. In this test, the fundamental signal (50 Hz) amplitude is also considered a drawback of the FOE-PID-GA regulator, which can be overcome in the future.

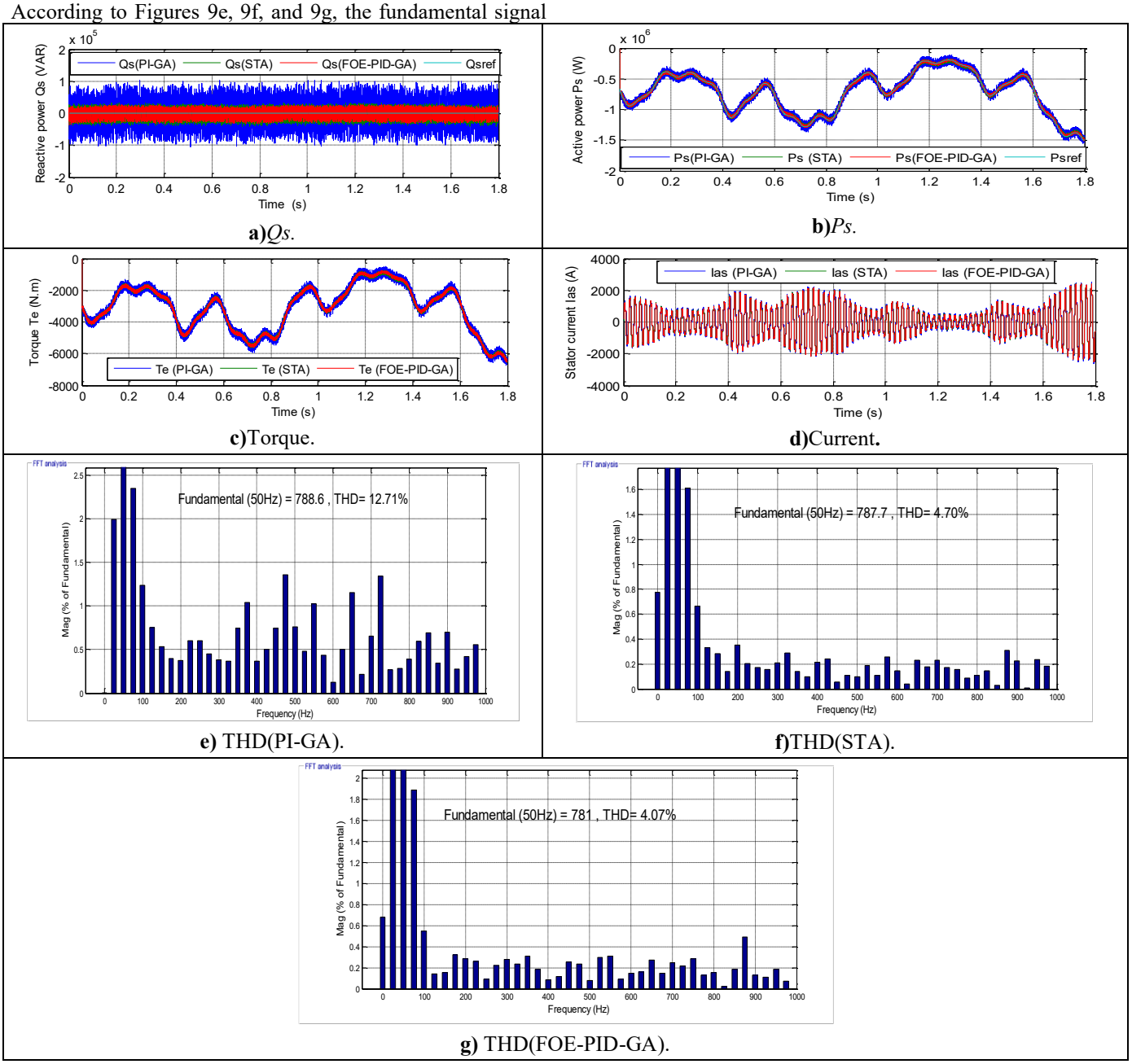

a) *Qs*.

b) *Ps*.

c) Torque.

d) Current.

e) THD(PI-GA).

f) THD(STA).

g) THD(FOE-PID-GA).

Fig. 9. Second test results.

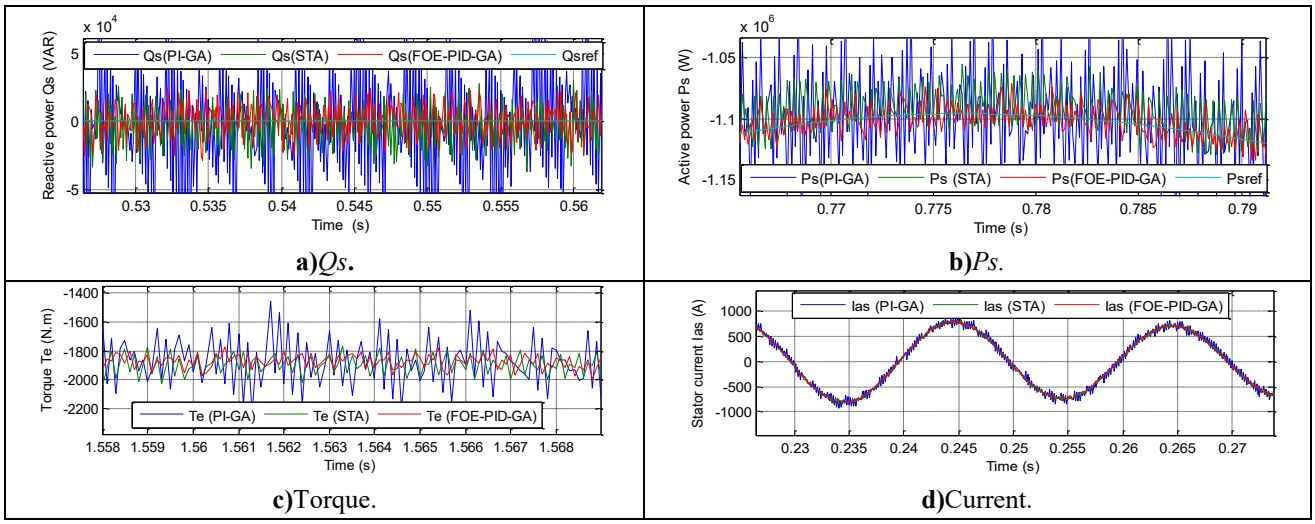

Fig. 10. Zoom (second test results).

Table 5. Values and reduction ratios in the second test case.

			Ps **(W)**	***Qs*** **(VAR)**
PI-GA	**Overshoot**		29530	15830
	Ripples		165020	200000
	ITAE		36080	34830
	Response time (ms)		0.66	0.07
	SSE		71800	40000
STA52	**Overshoot**		14940	17200
	Ripples		43950	57232
	ITAE		18100	13880
	Response time (ms)		1.65	0.20
	SSE		3700	16495
FOE-PID-GA	**Overshoot**		1440	18500
	Ripples		20000	40000
	ITAE		14450	12190
	Response time (ms)		2.09	0.46
	SSE		1100	1600
Ratios (%)	**Overshoot**	**FOE-PID/PI-GA**	95.12	16.49
		FOE-PID/STA	90.36	7.55
	Ripples	**FOE-PID/PI-GA**	87.88	80
		FOE-PID/STA	54.49	30.10
	ITAE	**FOE-PID/PI-GA**	59.95	65
		FOE-PID/STA	20.16	12.17
	Response time (ms)	**FOE-PID/PI-GA**	-68.42	-84.78
		FOE-PID/STA	-21.05	-56.52
	SSE	**FOE-PID/PI-GA**	98.46	96
		FOE-PID/STA	70.27	90.30

C. Third test: steps wind profile

The designed approach is tested against other strategies using steps WS profile. Figure 11a represents the WS variation pattern used in this test. This test differs from the tests performed above. The numerical results are presented in Table 6, while the graphical results are presented in Figure 11. A zoomed-in result for the third test is presented in Figure 12.

Figure 11b represents the change in reactive power for the three algorithms when using steps WS profile. From this figure, it is noticeable that this power closely follows the reference value, remaining constant at 0 VAR, which is the same as the results of the previous tests. Furthermore, it is noticeable that this power has a rapid dynamic response and ripples when using all three strategies. These ripples, as shown in Figure 12a, are larger when using the PI-GA controller than with other controllers. In this test, the FOE-PID-GA controller yielded significantly better numerical values for SSE, ripples, and ITAE of reactive power than both the PI-GA and STA controllers, as shown in Table 6. According to this table, the FOE-PID-GA regulator reduced the SSE, ripples, and ITAE of reactive power by 81.94%, 79.15%, and 68.29%, respectively, compared to the PI-GA regulator. Compared to the STA regulator, the FOE-PID-GA regulator reduced the SSE, ripples, and ITAE of reactive power by 67.79%, 28.53%, and 40.12%, respectively. However, the FOE-PID-GA

regulator yielded unsatisfactory values for both response time and overshoot of reactive power compared to other strategies. Therefore, it can be argued that response time and overshoot are also the drawbacks of this regulator design in this test.

Figure 11c represents the variation in active power in the third test case. For all three controls, it is observed that the active power varies with the change in WS, with a rapid dynamic response. It is also observed that the active power remains negative, with ripples present. These ripples, as shown in Figure 12b, are significantly lower in the case of the FOE-PID-GA controller compared to both the PI-GA and STA controllers.

Table 6 shows that the FOE-PID-GA regulator reduced active power ripples by 82.52% and 41.90% compared to the PI-GA and STA strategies, respectively. Furthermore, Table 6 shows that the FOE-PID-GA regulator achieved better ITAE, Overshoot, and SSE values, demonstrating its significant ability to improve active power characteristics compared to other strategies. Compared to the PI-GA controller, the FOE-PID-GA controller reduced the ITAE, Overshoot, and SSE values by 52.09%, 69.58%, and 87.90%, respectively. Furthermore, the designed controller reduced the ITAE, Overshoot, and SSE values by 11.25%, 61.58%, and 3.42%, respectively. Table 6 shows that the response time to active power of DFIG is significantly better with the PI-GA controller compared to the other controllers.

Figure 11d represents the torque variation over time for the three controls under steps WS conditions. This figure demonstrates that the torque continues to vary with the changes in the active power of the three controls. It is also noticeable that the torque has negative values and fluctuations. Figure 12c demonstrates that the torque ripples are significantly lower with the FOE-PID-GA controller compared to the other strategies. In the PI-GA model, the torque ripples were estimated at 400 N·m. Torque ripples were estimated at 237.46 N·m and 140 N·m for the STA and FOE-PID-GA models, respectively. Therefore, the FOE-PID-GA regulator reduced torque ripples by 65% and 41.04%, respectively. These results in this test demonstrate the effectiveness of the designed approach and its ability to improve torque quality, making it a reliable solution for industrial applications.

Figure 11e represents the current variation for the three algorithms in the third test. This figure demonstrates that the current takes the form of WS changes for the three controls, with ripples present. When using all three strategies, the current takes a sinusoidal shape, as shown in Figure 12d. According to Figure 12d, the current has a period of 0.02 seconds. The current ripples in this test were estimated to be 100 A, 20.42 A, and 5 A for the PI-GA, STA, and FOE-PID-GA, respectively. Therefore, the FOE-PID-GA regulator reduced current ripples by 79.58% and 75.51% compared to the PI-GA and STA, respectively.

Figures 11f, 11g, and 11h represent the THD values for the three controls in the third test case. In this test, the THD values were estimated to be 4.66%, 1.70%, and 1.29% for PI-GA, STA, and FOE-PID-GA, respectively. From these values, it is evident that the THD is lower for the FOE-PID-GA controller than for the other controllers. Thus, the FOE-PID-GA regulator reduced the THD value by 72.31% and 24.11% compared to the PI-GA and STA, respectively. Furthermore, it is noted that the fundamental signal (50 Hz) amplitude in this test was estimated to be 1058 A, 1064 A, and 1055 A for the PI-GA, STA, and FOE-PID-GA, respectively. It is noted that the FOE-PID-GA regulator yielded unsatisfactory amplitudes compared to other strategies. This disadvantage can be attributed to the low gain values, as the regulator's performance could be improved by using more efficient and effective strategies.

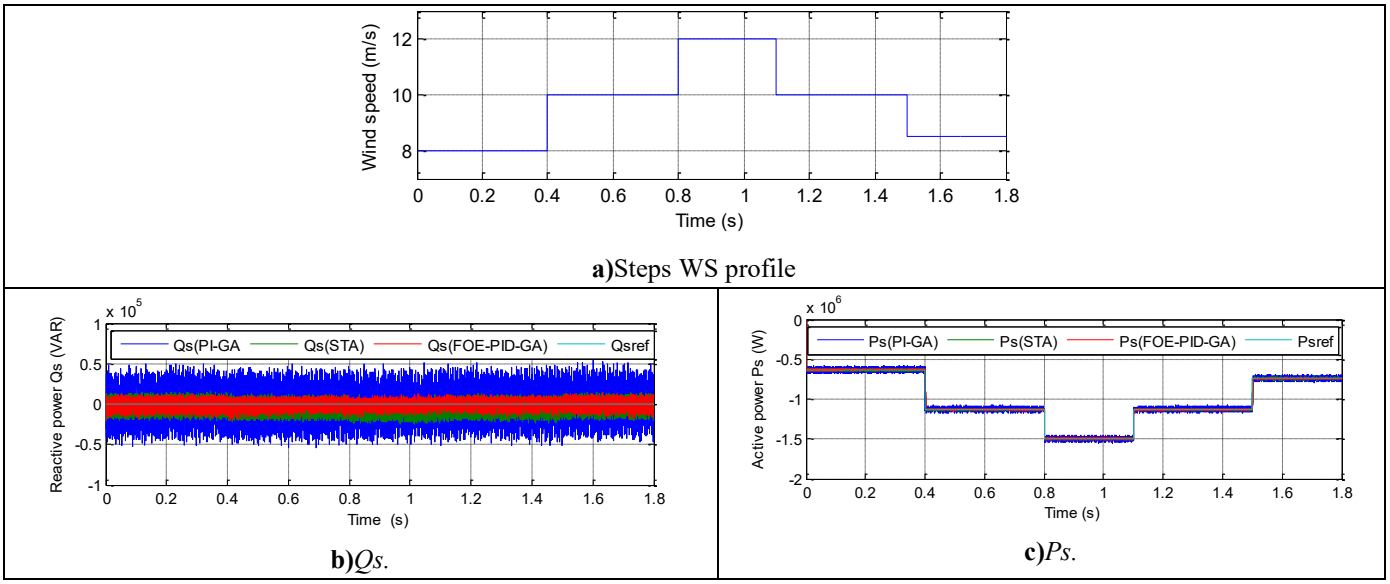

a)Steps WS profile

b)*Qs*.

c)*Ps*.

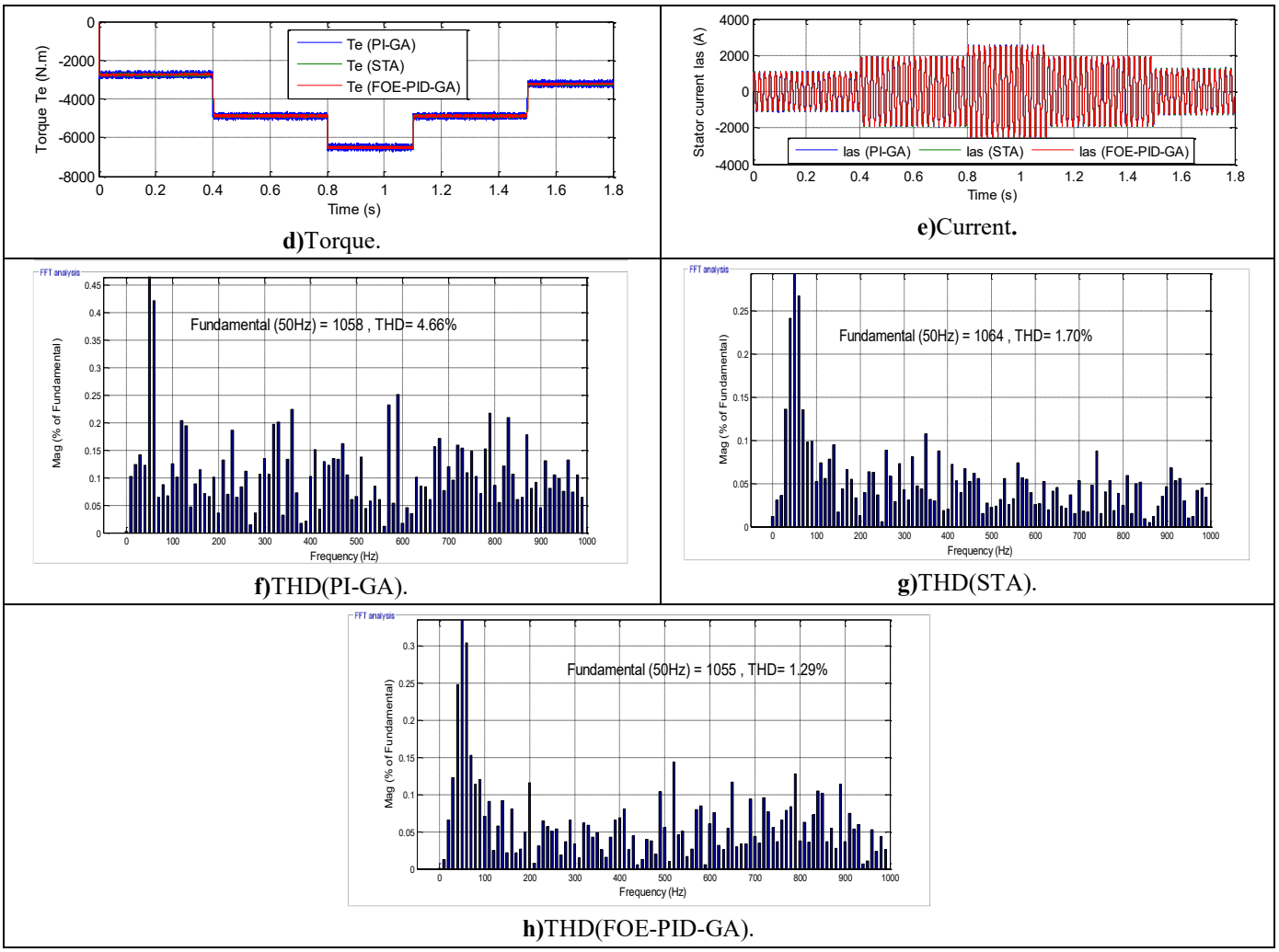

d)Torque. **e)**Current.

f)THD(PI-GA). **g)**THD(STA).

h)THD(FOE-PID-GA).

Fig. 11. Third test results.

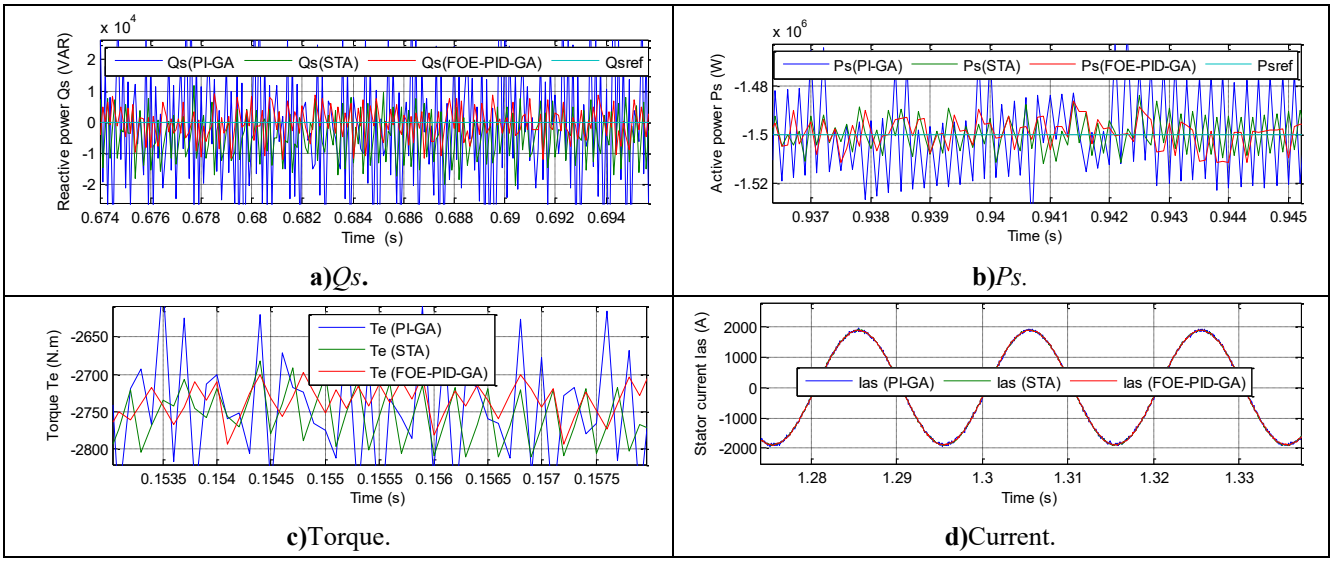

a)*Qs*. **b)***Ps*.

c)Torque. **d)**Current.

Fig. 12. First test results.

Table 6. Values and reduction ratios in the first test case.

			Qs **(VAR)**	***Ps*** **(W)**
PI-GA	**Overshoot**		8220	13350
	Ripples		103460	96500
	Response time (ms)		0.069	1.17
	ITAE		17500	18170
	SSE		22150	23310
ST55A	**Overshoot**		130.40	10570
	Ripples		30178	28620
	Response time (ms)		0.198	2.64
	ITAE		9276	9808
	SSE		12420	2920
FOE-PID-GA	**Overshoot**		10798	4060
	Ripples		21567	16860
	Response time (ms)		0.45	3.07
	ITAE		5554	8704
	SSE		4000	2820
Ratios (%)	**Overshoot**	**FOE-PID/PI-GA**	-23.87	69.58
		FOE-PID/STA	-98.79	61.58
	Ripples	**FOE-PID/PI-GA**	79.15	82.52
		FOE-PID/STA	28.53	41.90
	Response time (ms)	**FOE-PID/PI-GA**	-84.66	-61.88
		FOE-PID/STA	-57.77	-14
	ITAE	**FOE-PID/PI-GA**	68.26	52.09
		FOE-PID/STA	40.12	11.25
	SSE	**FOE-PID/PI-GA**	81.94	87.90
		FOE-PID/STA	67.79	3.42

D. Fourth test: without MPPT technique

In this test, the effectiveness and robustness of the designed approach are examined compared to the STA and PI-GA strategies when the MPPT strategy is not used. In this test, the reference active power value is set at a constant value of -800 kW. The results of this test are presented in Figures 13 and 14, while the numerical results are presented in Table 7.

Figures 13a and 13b represent the power changes over time for the fourth test. These powers track the reference well, with ripples. These ripples, as shown in Figures 14a and 14b, are lower with the FOE-PID-GA regulator than with both the STA and PI-GA regulators. Also, even though the MPPT strategy is not used, the *Qs* remains constant at 0, while the *Ps* remains constant at -800 kW. According to Table 7, the FOE-PID-GA regulator yielded better values for ITAE, ripples, and SSE of DFIG power compared to the other strategies. Compared to the STA regulator, the proposed regulator reduced the ripples, ITAE, and SSE of reactive power by 63.60%, 26.54%, and 40.07%, respectively. In the case of the PI-GA regulator, the proposed regulator reduced the ripples, ITAE, and SSE of *Qs* by 63.60%, 26.54%, and 40.07%, respectively.

In the *Ps* case, the ripples, ITAE, overshoot, and SSE values are significantly improved with the designed regulator, with ratios of 86.41%, 67.45%, 61.50%, and 77.38%, respectively, compared to the PI-GA regulator. Compared to the STA regulator, the FOE-PID-GA regulator reduced ripples, ITAE, and SSE by 49.36%, 39.35%, and 31.39%, respectively. Regarding the power response time, Table 7 shows that the FOE-PID-GA regulator yielded an unsatisfactory response time compared to the other strategies, which suggests that the power response time is also a drawback of this approach in this test.

Figures 13c and 13d represent the variations in torque and current for the three controls in the fourth test case. From these figures, it is observed that the torque and current vary with the change in *Ps*, with ripples present. These ripples, as shown in Figures 14c and 14d, are lower in the case of the FOE-PID-GA regulator compared to the other strategies. The torque ripples in the test were estimated to be 300 N.m, 70 N.m, and 40 N.m for the PI-GA, STA, and FOE-PID-GA, respectively. Therefore, the FOE-PID-GA regulator reduced torque ripples by 86.66% and 42.85% compared to the PI-GA and STA, respectively. Meanwhile, the current ripples in this test were estimated at 108.50 A, 38.10 A, and 20 A for the PI-GA, STA, and FOE-PID-GA, respectively. These values indicate that the FOE-PID-GA regulator reduced current ripples by 81.56% and 47.50% compared to the PI-GA and STA, respectively. These ratios prove the effectiveness of the designed regulator despite not using the MPPT strategy, as these results confirm the results of the above tests.

Figures 13e, 13f, and 13g represent the THD of current values for the three controllers used in this paper. Based on these figures, the THD values were estimated to be 3.63%, 1.32%, and 1.07% for PI-GA, STA, and FOE-PID-GA, respectively. Therefore, the FOE-PID-GA regulator reduced the THD value by 70.52% and 18.93 % compared to the PI-GA and STA, respectively. Therefore, the current quality is high in this test when using the designed regulator compared to the other strategies. However, in terms of the fundamental signal (50 Hz) amplitude, this regulator gave an unsatisfactory amplitude. Therefore, this amplitude value is also considered a negative for the designed approach in this test.

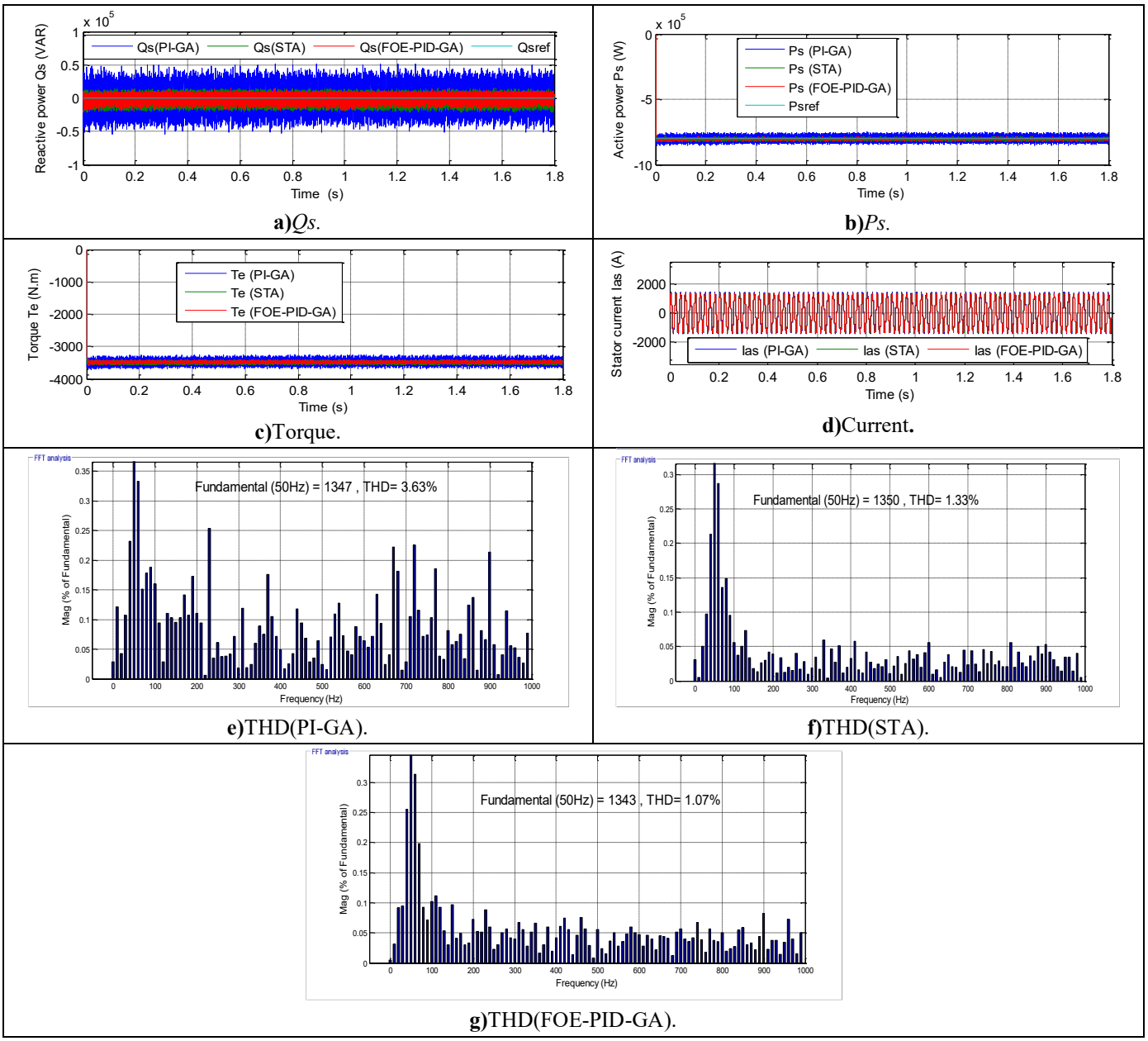

Fig. 13. Fourth test results.

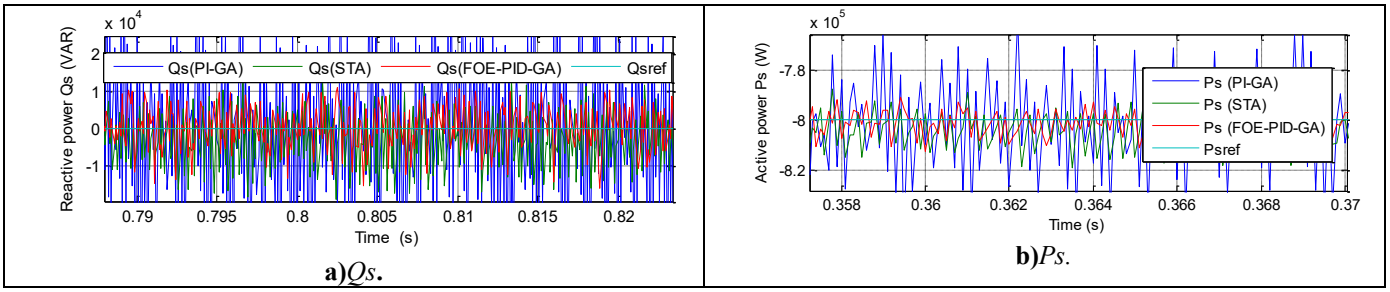

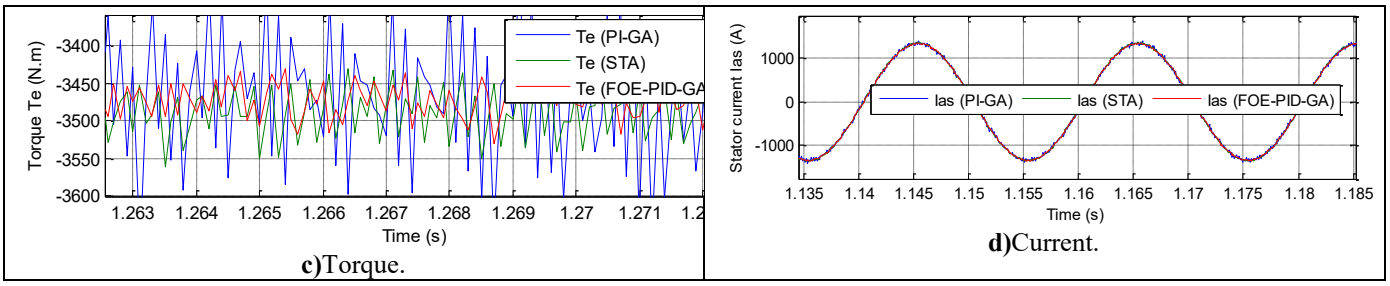

c)Torque. **d)**Current.

Fig. 14. Fourth test results.

Table 7. Values and reduction ratios in the fourth test case.

			***Qs* (VAR)**	***Ps* (W)**
PI-GA	**Overshoot**		8213	14190
	Ripples		101232	88130
	Response time (ms)		0.069	1.66
	ITAE		17130	16830
	SSE		14556	26350
ST57A	**Overshoot**		130.50	4570
	Ripples		30000	23700
	Response time (ms)		0.19	3.47
	ITAE		8009	9031
	SSE		2600	8760
FOE-PID-GA	**Overshoot**		10798	5500
	Ripples		10917.50	12000
	Response time (ms)		0.40	4.09
	ITAE		5883	5477
	SSE		1558	5960
Ratios (%)	**Overshoot**	**FOE-PID/PI-GA**	-23.93	61.50
		FOE-PID/STA	-98.79	-16.90
	Ripples	**FOE-PID/PI-GA**	89.21	86.41
		FOE-PID/STA	63.60	49.36
	Response time (ms)	**FOE-PID/PI-GA**	-82.75	-59.41
		FOE-PID/STA	-52.50	-15.15
	ITAE	**FOE-PID/PI-GA**	65.65	67.45
		FOE-PID/STA	26.54	39.35
	SSE	**FOE-PID/PI-GA**	89.29	77.38
		FOE-PID/STA	40.07	31.96

Table 8 compares the THD value with related studies. The new algorithm significantly minimized the THD value in two tests compared to several papers, confirming the efficacy of this algorithm and its high ability to enhance current quality. In the first test case, the new algorithm reduced the THD compared to [93], [94], [95], and [97] by 47.16%, 60.09%, 26.25%, and 63.50%, respectively. In the second test case, the new algorithm reduced the THD value compared to [93], [94], [95], and [97] by 41.94%, 56.14%, 18.95%, and 59.89%, respectively. These ratios demonstrate the efficacy of the new algorithm in enhancing current quality despite changes in generator parameters, making it a highly valuable solution for the future. The obtained minimization ratios are graphically represented in Figure 15. From Figure 15, the largest reduction ratio in the test case was estimated at 70.50%, while the lowest reduction ratio achieved was estimated at 12.59%.

Figure 15 also shows that in the second test case, the largest reduction percentage was in the case of comparison with work [96], where this percentage was estimated at 67.58%. The lowest reduction percentage obtained in the second test was in comparison with work [92], where it was estimated at 3.95%. Therefore, the lowest and highest minimization ratios in the first test were greater than the lowest and highest reduction ratios in the second test, which indicates that the effectiveness of the new algorithm is greater when the system is operating normally.

As shown in Table 8, the proposed FOE-PID-GA control strategy achieves a lower THD compared with the other methods reported in the literature. This improvement can be attributed to the enhanced flexibility of the FOE, which provides additional tuning parameters beyond those available in conventional integer-order controllers. This flexibility allows a more accurate adjustment of the system dynamic response and improves the tracking performance of the control loops. Furthermore, the use of the GA method enables an

optimal tuning of the controller parameters by exploring a wider search space and avoiding local minima. As a result, the proposed FOE-PID-GA controller reduces current oscillations and improves the quality of the converter output waveform, leading to a significant reduction in THD compared with the existing control strategies.

Table 8. Comparison with other papers in terms of THD values.

References	Methods	THD (%)	Ratios (%)	
			Test 1	Test 2
[92]	Method 1	4.05	12.59	3.95
	Method 2	10.79	67.19	63.94
[93]	DTC	6.70	47.16	41.94
[94]	DPC	8.87	60.09	56.14
[95]	GA-based DTC	4.80	26.25	18.95
[96]	Algorithm 1	7.19	50.76	45.89
	Algorithm 2	12	70.50	67.58
[97]	Integral SMC	9.7	63.50	59.89
[98]	Control 1	4.19	15.51	7.15
	Control 2	4.88	27.45	20.28
New algorithm	Test 1	3.54	-	
	Test 2	3.89		

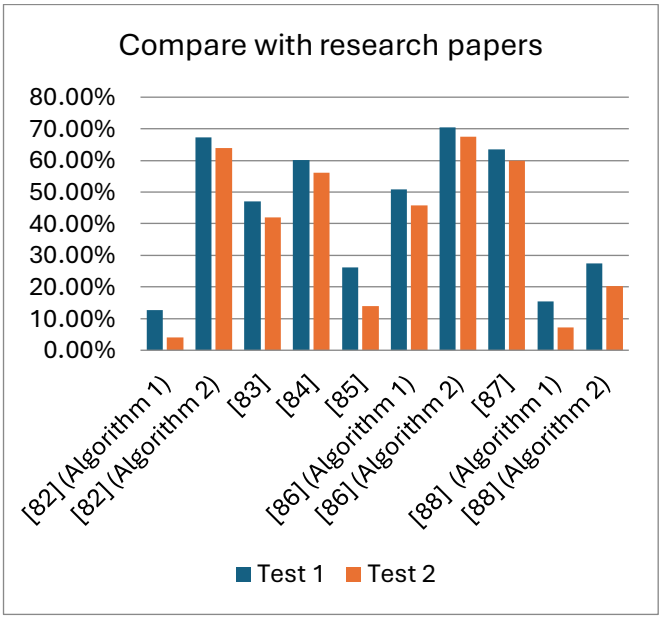

Fig. 15. Graph of the results comparing with other related studies.

5. Conclusion

To enhance the quality of the power output of a DFIG-based power system, this work presents a new power control algorithm. The FOE-PID-GA algorithm is used as a suitable solution to increase competence and improve current and power quality. A genetic algorithm is used to fine-tune the parameters of the designed regulator. Furthermore, the effectiveness of the new algorithm is evaluated under uncertainties and wind speed variations, comparing its performance with that of the PI-GA regulator. In all tests conducted, numerical and graphical results demonstrate that the new algorithm outperforms the PI-GA regulator. This superiority is evident in the reduction of power ripples, where, in the robustness test, active power ripples were reduced by 68.83%. In all tests, the THD of the current was reduced by 20% and 25% compared to PI-GA, thereby enhancing the overall quality of the power grid. The new algorithm also significantly improves the SSE value for active power by 97.01% and 74.52% in all tests. Given the simplicity and ease of realization of the designed algorithm, it can be used in solar energy systems, providing a promising future direction. Moving to practical work by conducting experiments on a small-scale wind turbine system will help verify the applicability and performance of the new algorithm in the real world. Working with energy sector partners to conduct field tests on large-scale wind turbine systems to evaluate the performance of the new algorithm under a variety of operating settings. These field tests help identify any unique challenges in real-world deployments. It is recommended to investigate dynamically adjusting regulator gains in response to changing operating conditions using advanced optimization strategies, such as forced learning methods, adaptive optimization methods, or evolutionary methods. Using a novel algorithm to conduct a comprehensive investigation into the environmental impacts of multi-rotor wind turbine systems, taking into account sustainable wind farm development, life cycle, and carbon footprint analyses.

Nomenclature

WP	Wind power
PI	Proportional integral controller
WS	Wind speed
THD	Total harmonic distortion
DPC	Direct vector control
FOE	Fractional-order error
MRWT	Multi-rotor wind turbine
Ps	Active power
DFIG	Doubly-fed induction generator
LVRT	Low-voltage ride-through
STA	Super-twisting algorithm
MSC	Machine-side converter
MRAC	Model reference adaptive control
ADRC	Active disturbance rejection control
DVC	Direct vector control
MLC	Multilevel converter
ANFIS	Adaptive neuro-fuzzy inference system
PSO	Particle swarm optimization
GWO	Gray Wolf optimization
HAWT	Herizontal-axis wind turbine
PSMC	Prescribed sliding mode control
WT	Wind turbine
NN	Neural network

BC	Backstepping control
VAWT	Vertical-axis wind turbine
GA	Genetic Algorithm
FRT	Fault-ride-through
SSE	Steady-state error
GSC	Grid-side converter
HOSMC	High-order sliding mode control
MRAS	Model reference adaptive system
MPC	Model predictive control
SWA	Salp Swarm algorithm
FLC	Fuzzy logic control
MMLC	Modular multilevel converter
ITAE	Integral of time-weighted absolute error
WOA	Whale optimization algorithm
SMC	Sliding mode control

Funding

Not applicable.

Data Availability

Data available on request from the authors. The datasets used and/or analysed during the current study available from the corresponding author on reasonable request. In the event of communication, the fist author (Habib Benbouhenni,

E-mail: [h.benbouhenni@univ-chlef.dz](mail to: h.benbouhenni@univ-chlef.dz)) will respond to any inquiry or request.

Author Contributions

Conceptualization, H.B.; methodology, H.B., F. A., and N.B.; software, H.B.; validation, H.B.; formal analysis, H.B. and N.B.; investigation, H.B. and N.B.; resources, H.B.; data curation, H.B.; writing—original draft preparation, N.B., F. A., and H.B.; writing—review and editing, H.B. and N.B.; visualization, H.B., F.A., and N.B.; supervision, H.B., F.A., and N.B.; project administration, H.B.; funding acquisition, N.B. and H.B. All authors have read and agreed to the published version of the manuscript.

Conflict of Interest

The authors declare no conflict of interest.

References

[1] B. Alexander, "Wind industry installs record capacity in 2024 despite policy instability," Global Wind Energy Council (GWEC), Reports, 2025. [Online]. Available: https://www.gwec.net/gwec-news/wind-industry-installs-record-capacity-in-2024-despite-policy-instability

[2] M. Sidhi, "Global wind installations hit record highs in 2024, but policy gaps loom large," Global Wind Report 2025, 2025.

[3] S. I. Ahmad, K. Nqibullah, M. H. Elkholy, A. L. Gul, E. Said, H. Ahmadullah, T. S., M. G. Mahmoud, and G. P., "Techno-economic evaluation and comparison of the optimal PV/Wind and grid hybrid system with horizontal and vertical axis wind turbines," Energy Conversion and Management: X, vol. 23, p. 100638, 2024. doi: https://doi.org/10.1016/j.ecmx.2024.100638

[4] T. Abhishiktha, K. V. Ratna, K. S. Dipankur, V. Indraja, and K. V. Hari, "A review on small scale wind turbines," Renewable and Sustainable Energy Reviews, vol. 56, pp. 1351–1371, 2016. doi: https://doi.org/10.1016/j.rser.2015.12.027

[5] Y. Ibrahim, S. Abdelhafid, and P. Wira, "Control of doubly-fed induction generator using artificial neural network controller," Revue Roumaine des Sciences Techniques – Série Électrotechnique et Énergétique, vol. 68, no. 1, pp. 46–51, 2023.

[6] S. K. G. Sanjeev, M. Sundram, and S. Madhu, "Performance enhancement of DFIG based grid connected SHPP using ANN controller," International Journal of Renewable Energy Research, vol. 9, no. 3, pp. 1165–1179, 2019. doi: https://doi.org/10.20508/ijrer.v9i3.9427.g7694

[7] S. A. Dayo, A. Memon, Z. A. Memon et al., "A new approach for improving dynamic fault ride through capability of grid-tied based wind turbines," Scientific Reports, vol. 15, p. 6144, 2025. doi: https://doi.org/10.1038/s41598-025-89396-0

[8] Z. Dao, F. Blaabjerg, T. Franke, M. Thøgersen, and M. Liserre, "Comparison of wind power converters reliability with low-speed and medium-speed permanent magnet synchronous generators," IEEE Transactions on Industrial Electronics, vol. 62, no. 10, pp. 6575–6584, 2015. doi: https://doi.org/10.1109/TIE.2015.2447502

[9] S. Rajendran, M. Diaz, R. Cárdenas, E. Espina, E. Contreras, and J. Rodriguez, "A review of generators and power converters for multi-MW wind energy conversion systems," Processes, vol. 10, pp. 2302, 2022. doi: https://doi.org/10.3390/pr10112302

[10] H. C. Hüseyin, A. Demir, and Y. Oner, "Investigation of dynamic behavior of double feed induction generator and permanent magnet synchronous generator wind turbines in failure conditions," International Journal of Renewable Energy Research, vol. 11, no. 2, pp. 721–729, 2021. doi: https://doi.org/10.20508/ijrer.v11i2.11837.g8193

[11] T. Benali, A. S. Islam, and D. K. Ibrahim, "Performance enhancement of doubly-fed induction generator-based wind energy system," International Journal of Renewable Energy Research, vol. 13, no. 1, pp. 311–325, 2023. doi: https://doi.org/10.20508/ijrer.v13i1.13649.g8685

[12] H. Benbouhenni, "Application of STA methods and modified SVM strategy in direct vector control system of ASG integrated to dual-rotor wind power: Simulation studies," International Journal of Smart Grid, vol. 5, no. 1, pp. 63–73, 2021. doi: https://doi.org/10.20508/ijsmartgrid.v5i1.173.g136

[13] H. Benbouhenni, "Rotor flux and electromagnetic torque regulation of DFIG using dual PI controllers," International Journal of Smart Grid, vol. 7, no. 4, pp. 227–234, 2023. doi: https://doi.org/10.20508/ijsmartgrid.v7i4.308.g311

[14] W. Wojtkowski and R. Kociszewski, "Pulse-width modulation approaches for efficient harmonic suppression," Electronics, vol. 14, p. 2651, 2025. doi: https://doi.org/10.3390/electronics14132651

[15] H. Othman, M. Allagui, and B. Jamel, "Direct drive wind turbine equipped with an active and reactive power supervisory," International Journal of Renewable Energy Research, vol. 4, no. 2, pp. 435–444, 2014. doi: https://doi.org/10.20508/ijrer.v4i2.1244.g6296

[16] E. Aboubakr, E. Yassir, B. Youness, E. Hassane, and E. Hassan, "LVRT control strategy of DFIG based wind turbines combined with active and passive protections," International Journal of Renewable Energy Research, vol. 7, no. 3, pp. 1258–1269, 2017. doi: https://doi.org/10.20508/ijrer.v7i3.6014.g7159

[17] J. Hu, Y. Chen, X. Tang, Y. Li, Y. Xu, and F. Chen, "A survey on development and prospect of wind turbines virtual synchronous control technology," Energy Reports, vol. 8, pp. 75–83, 2022. doi: https://doi.org/10.1016/j.egyr.2021.11.005

[18] W. M. Kermiche, E. B., A. B. D., F. S., B. B., and I. Colak, "Maximizing wind power efficiency with hybrid excitation synchronous generators and energy storage systems through advanced control strategies," Journal of Energy Storage, vol. 109, p. 115219, 2025. doi: https://doi.org/10.1016/j.est.2024.115219.

[19] A. Dridi, J. H., M. A., M. Ch., and H. Trabelsi, "Robust fractional PI controller design for stand-alone microgrid under load variation: An optimization-based approach," International Journal of Renewable Energy Research, vol. 13, no. 4, pp. 1526–1537, 2023. doi: https://doi.org/10.20508/ijrer.v13i4.14540.g8826

[20] V. Phuong, T. D. Anh, and N. A. Linh, "A novel multi-step model predictive control design for three-phase T-type inverter in grid-connected mode," International Journal of Renewable Energy Research, vol. 11, no. 4, pp. 1968–1976, 2021. doi: https://doi.org/10.20508/ijrer.v11i4.12481.g8353

[21] H. Benbouhenni and H. Gasmi, "Comparative study of synergetic controller with super twisting algorithm for rotor side inverter of DFIG," International Journal of Smart Grid, vol. 6, no. 4, pp. 144–156, 2022. doi: https://doi.org/10.20508/ijsmartgrid.v6i4.265.g251

[22] S. Messaoudi, A. Elharif, N. Tamou, and B. B. Ibrahim, "An efficient nonlinear backstepping controller approach of a wind energy conversion system based on a DFIG," International Journal of Renewable Energy Research, vol. 7, no. 4, pp. 1520–1528, 2017. doi: https://doi.org/10.20508/ijrer.v7i4.6112.g7192

[23] H. Benbouhenni and H. Gasmi, "Comparative study of synergetic controller with super twisting algorithm for rotor side inverter of DFIG," International Journal of Smart Grid, vol. 6, no. 4, pp. 144–156, 2022. doi: https://doi.org/10.20508/ijsmartgrid.v6i4.265.g228

[24] F. B. Fatma, A. M. Abdelkarim, A. A. Achraf, and L. K. Lotfi, "Coordinated control of SMES and DVR for improving fault ride-through capability of DFIG-based wind turbine," International Journal of Renewable Energy Research, vol. 12, no. 1, pp. 359–371, 2022. doi: https://doi.org/10.20508/ijrer.v12i1.12681.g8410.

[25] A. Baltag, G. Livint, A. G. Baciu, and S. Bellarbi, "Design of H∞ robust controllers for wind turbines based on DFIG," in International Conference and Exposition on Electrical and Power Engineering (EPE), Iași, Romania, 2022, pp. 187–192. doi: 10.1109/EPE56121.2022.9959784

[26] D. Li and J. Dong, "Fuzzy weight-based reinforcement learning for event-triggered optimal backstepping control of fractional-order nonlinear systems," IEEE Transactions on Fuzzy Systems, vol. 32, no. 1, pp. 214–225, 2024. doi: 10.1109/TFUZZ.2023.3294928

[27] D. Li and J. Dong, "Fractional-order systems optimal control via actor-critic reinforcement learning and its validation for chaotic MFET," IEEE Transactions on Automation Science and Engineering, vol. 22, pp. 1173–1182, 2025. doi: 10.1109/TASE.2024.3361213

[28] D. Li and J. Dong, "Approximate optimized backstepping control of uncertain fractional-order nonlinear systems based on reinforcement learning," IEEE Transactions on Systems, Man, and Cybernetics: Systems, vol. 54, no. 11, pp. 6723–6732, 2024. doi: 10.1109/TSMC.2024.3426923

[29] A. A. Thirthar, A. L. Alaoui, S. Roy et al., "Fractional and stochastic dynamics of predator–prey systems: The role of fear and global warming," European Physical Journal B, vol. 98, p. 147, 2025. doi: https://doi.org/10.1140/epjb/s10051-025-00992-5

[30] U. Ghosh, A. A. Thirthar, B. Mondal et al., "Effect of fear, treatment, and hunting cooperation on an eco-epidemiological model: Memory effect in terms of fractional derivative," Iran Journal of Science and Technology, Transactions of Science, vol. 46, pp. 1541–1554, 2022. doi: https://doi.org/10.1007/s40995-022-01371-w.

[31] A. A. Th. Ashraf, A. Hamadjam, A. L. Abdesslem, and S. N. Kottakkaran, "Dynamical behavior of a fractional-order epidemic model for investigating two fear effect functions," Results in Control and Optimization, vol. 16, p. 100474, 2024. doi: https://doi.org/10.1016/j.rico.2024.100474

[32] A. A. Thirthar, S. K. N., B. Mondal et al., "Utilizing memory effects to enhance resilience in disease-driven prey–predator systems under the influence of global

warming," Journal of Applied Mathematics and Computation, vol. 69, pp. 4617–4643, 2024. doi: https://doi.org/10.1007/s12190-023-01936-x

[33] A. A. Th. Ashraf, P. Prabir, K. Aziz, A. A. Manar, and A. Thabet, "An ecosystem model with memory effect considering global warming phenomena and an exponential fear function," Fractals, vol. 31, no. 10, p. 2340162, 2023. doi: https://doi.org/10.1142/S0218348X2340162X

[34] N. Samala and C. Bethi, "Enhancing the performance and integrity of grid-tied green power systems using unified power quality conditioner and fractional order control," International Journal of Renewable Energy Research, vol. 14, no. 4, pp. 814–823, 2024. doi: https://doi.org/10.20508/ijrer.v14i4.14673.g8965

[35] I. K. Indrajit, A. Das, and G. K. Panda, "Wind energy infiltrated multi-area power system: Optimized 2-DOF-FOPID controller for LFC," International Journal of Renewable Energy Research, vol. 12, no. 2, pp. 743–756, 2020.

[36] M. Mamashli and M. Jamil, "Enhanced dynamic control for flux-switching permanent magnet machines using integrated model predictive current control and sliding mode control," Energies, vol. 18, pp. 1061, 2025. doi: https://doi.org/10.3390/en18051061

[37] T. Messaoud, A. Ghouili, R. Boushaki, T. M. B., D. Kermadi, M. B., M. Ch., and V. Blahnik, "Sensorless finite set predictive current control with MRAS estimation for optimized performance of standalone DFIG in wind energy systems," Results in Engineering, vol. 24, pp. 103622, 2024. doi: https://doi.org/10.1016/j.rineng.2024.103622

[38] H. Hamdi, A. Marii, C. Ben Regaya, and A. Zaafouri, "A robust approach to an adaptive gain sliding mode controller based on MRAC of a wind power conversion system based on a DFIG," in International Conference on Control, Decision and Information Technologies (CoDIT), Valletta, Malta, 2024, pp. 1323–1328. doi: 10.1109/CoDIT62066.2024.10708130.

[39] H. Meneses, O. Arrieta, F. Padula, A. Visioli, and R. Vilanova, "FOPI/FOPID tuning rule based on a fractional order model for the process," Fractal and Fractional, vol. 6, pp. 478, 2022. doi: https://doi.org/10.3390/fractalfract6090478

[40] M. Chakib, N. Tamou, and A. Elharif, "Contribution of variable speed wind turbine generator based on DFIG using ADRC and RST controllers to frequency regulation," International Journal of Renewable Energy Research, vol. 11, no. 1, pp. 320–331, 2021.

[41] C. R. Reddy, K. Naresh, P. U. Reddy, and P. Sujatha, "Control of DFIG based wind turbine with hybrid controllers," International Journal of Renewable Energy Research, vol. 10, no. 3, pp. 1488–1500, 2020. doi: https://doi.org/10.20508/ijrer.v10i3.11010.g8028

[42] V. Lakshmi Narayanan and R. Ramakrishnan, "Pitch control of a digital hydraulics pitch system for wind turbine based on neuro-fuzzy digital pitch controller," International Journal of Renewable Energy Research, vol. 11, no. 1, pp. 416–425, 2021. doi: https://doi.org/10.20508/ijrer.v11i1.11626.g8153

[43] A. V. Hemeyine, A. Abbou, A. Bakouri, M. Mokhlis, and S. M. El Moustapha, "A robust interval type-2 fuzzy logic controller for variable speed wind turbines based on a doubly fed induction generator," Inventions, vol. 6, p. 21, 2021. doi: https://doi.org/10.3390/inventions6020021

[44] A. Q. Adnan, M. K. H. Mohammed, A. M. Ardashir, and K. S. Kamran, "Optimal hybrid type-3 fuzzy controller for horizontal axis wind turbines: Comparative study," ISA Transactions, vol. 161, pp. 200–215, 2025. doi: https://doi.org/10.1016/j.isatra.2025.03.025

[45] H. Benbouhenni, N. Bizon, M. Yessef et al., "Experimental analysis of genetic algorithm-enhanced PI controller for power optimization in multi-rotor variable-speed wind turbine systems," Scientific Reports, vol. 15, p. 1407, 2025. doi: https://doi.org/10.1038/s41598-024-81281-6

[46] S. A. Dayo, A. Memon, Z. A. Memon et al., "A new approach for improving dynamic fault ride through capability of grid-tied based wind turbines," Scientific Reports, vol. 15, p. 6144, 2025. doi: https://doi.org/10.1038/s41598-025-89396-0

[47] F. Lu and D. Gerling, "Multi-objective optimization for DFIG based wind energy conversion system by using NSGA-II," in International Conference on Electrical Machines and Systems (ICEMS), Harbin, China, 2019, pp. 1–6. doi: 10.1109/ICEMS.2019.8921548.

[48] H. Benbouhenni and N. Bizon, "Advanced direct vector control method for optimizing the operation of a double-powered induction generator-based dual-rotor wind turbine system," Mathematics, vol. 9, pp. 2403, 2021. doi: https://doi.org/10.3390/math9192403

[49] M. Hermassi, S. Krim, Y. Kraiem et al., "Design of vector control strategies based on fuzzy gain scheduling PID controllers for a grid-connected wind energy conversion system: Hardware FPGA-in-the-loop verification," Electronics, vol. 12, pp. 1419, 2023. doi: https://doi.org/10.3390/electronics12061419

[50] H. Benbouhenni, Y. Mourad, N. Bizon et al., "Hardware-in-the-loop simulation to validate the fractional-order neuro-fuzzy power control of variable-speed dual-rotor wind turbine systems," Energy Reports, vol. 11, pp. 4904–4923, 2024. doi: https://doi.org/10.1016/j.egyr.2024.04.049

[51] A. Khedher, N. K. Nihel, and M. F. Mohamed, "Wind energy conversion system using DFIG controlled by backstepping and sliding mode strategies," International Journal of Renewable Energy Research, vol. 2, no. 3, pp.

421–434, 2012. doi: https://doi.org/10.20508/ijrer.v2i3.249.g6040

[52] A. P. Shah and A. J. Mehta, "Direct power control of DFIG using super-twisting algorithm based on second-order sliding mode control," in International Workshop on Variable Structure Systems (VSS), Nanjing, China, 2016, pp. 136–141. doi: 10.1109/VSS.2016.7506905.

[53] K. Ma, R. Wang, H. Nian, X. Wang, and W. Fan, "Nonlinear model predictive control for doubly fed induction generator with uncertainties," Applied Sciences, vol. 14, pp. 1818, 2024. doi: https://doi.org/10.3390/app14051818

[54] H. Nusrat and S. M. U. A. Syed, "On integration of wind power into existing grids via modular multilevel converter based HVDC systems," International Journal of Renewable Energy Research, vol. 10, no. 3, pp. 1060–1070, 2020. doi: https://doi.org/10.20508/ijrer.v10i3.10638.g7980

[55] H. Alnuman, E. Hussain, M. Aly et al., "Cascaded H-bridge multilevel converter topology for a PV connected to a medium-voltage grid," Machines, vol. 13, p. 540, 2025. doi: https://doi.org/10.3390/machines13070540

[56] A. Benevieri, S. Cosso, A. Formentini et al., "Advances and perspectives in multilevel converters: A comprehensive review," Electronics, vol. 13, p. 4736, 2024. doi: https://doi.org/10.3390/electronics13234736

[57] L. Zhao et al., "Fast simulation of MMC-HVDC systems using a generalized equivalent circuit model of MMC," in IEEE International Conference on Control and Automation (ICCA), Singapore, 2020, pp. 1605–1611. doi: 10.1109/ICCA51439.2020.9264378.

[58] A. Redouane, R. Saou, and A. Oukaour, "Flying capacitor voltage balancing control strategy based on logic equations in five-level ANPC inverter," Periodica Polytechnica Electrical Engineering and Computer Science, vol. 67, no. 4, pp. 438–448, 2023. doi: https://doi.org/10.3311/PPee.21879

[59] M. Elrheem and N. K. B. Naglaa, "A comparison between using a firefly algorithm and a modified PSO technique for stability analysis of a PV system connected to grid," International Journal of Smart Grid, vol. 1, no. 1, pp. 1–8, 2017. doi: https://doi.org/10.20508/ijsmartgrid.v1i1.1.g1

[60] J. Tang and L. Wang, "A whale optimization algorithm based on atom-like structure differential evolution for solving engineering design problems," Scientific Reports, vol. 14, pp. 795, 2024. doi: https://doi.org/10.1038/s41598-023-51135-8.

[61] K. U. Z. Zaman, K. Naveed, and A. A. Kumar, "Tuning of PID controller using whale optimization algorithm for different systems," in Proc. International Conference on Digital Futures and Transformative Technologies (ICoDT2), Islamabad, Pakistan, 2021, pp. 1–5, doi: 10.1109/ICoDT252288.2021.9441526.

[62] Y. L. A. Sumanth, L. Lakshminarasimman, and G. Sambasiva Rao, "Optimal design of FOPID controller for DFIG-based wind energy conversion system using grey-wolf optimization algorithm," International Journal of Renewable Energy Research, vol. 12, no. 4, pp. 2111–2120, 2022, doi: 10.20508/ijrer.v12i4.13446.g8594.

[63] H. Benbouhenni and S. Lemdani, "Combining synergetic control and super twisting algorithm to reduce the active power undulations of doubly fed induction generator for dual-rotor wind turbine system," Electrical Engineering & Electromechanics, no. 3, pp. 8–17, 2021, doi: 10.20998/2074-272X.2021.3.02.

[64] H. Benbouhenni, N. Bizon, M. Yessef et al., "Experimental analysis of genetic algorithm-enhanced PI controller for power optimization in multi-rotor variable-speed wind turbine systems," Scientific Reports, vol. 15, pp. 1407, 2025, doi: 10.1038/s41598-024-81281-6.

[65] N. Mohamed, E. Ahmed, and N. Tamou, "Comparative analysis between PI and backstepping control strategies of DFIG driven by wind turbine," International Journal of Renewable Energy Research, vol. 7, no. 3, pp. 1307–1316, 2021.

[66] S. Kadi, K. Imarazene, E. M. Berkouk, M. Horch, and E. Abdelkarim, "High order sliding mode of connected DFIG-variable speed wind turbine," in Proc. International Multi-Conference on Systems, Signals & Devices (SSD), Sétif, Algeria, 2022, pp. 1275–1280, doi: 10.1109/SSD54932.2022.9955975.

[67] S. Wang, J. Zhou, and Z. Duan, "Finite frequency H∞ control for doubly fed induction generators with input delay and gain disturbance," Sustainability, vol. 15, p. 4520, 2023, doi: 10.3390/su15054520.

[68] A. Kaneko, N. Hara, and K. Konishi, "Model predictive control of DFIG-based wind turbines," in Proc. American Control Conference (ACC), Montreal, QC, Canada, 2012, pp. 2264–2269, doi: 10.1109/ACC.2012.6314883.

[69] K. Narimene, M. Kheira, and F. Mohamed, "Robust neural control of wind turbine based doubly fed induction generator and NPC three-level inverter," Periodica Polytechnica Electrical Engineering and Computer Science, vol. 66, no. 2, pp. 191–204, 2022, doi: 10.3311/PPee.19921.

[70] R. Rouabhi, A. Herizi, and A. Djerioui, "Performance of robust type-2 fuzzy sliding mode control compared to various conventional controls of doubly-fed induction generator for wind power conversion systems," Energies, vol. 17, p. 3778, 2024, doi: 10.3390/en17153778.

[71] T. Aounallah, N. Ferhat, N. Essounbouli, and A. Hamzaoui, "A new fractional-order adaptive interval type-3 fuzzy logic-backstepping control algorithm of doubly fed induction generators," IEEE Access, vol. 13, pp. 95445–95456, 2025, doi: 10.1109/ACCESS.2025.3575048.

[72] M. E. Abdallah, O. M. Arafa, A. Shaltot, and G. A. Abdel-Aziz, "MRAC-based vector oriented control of a wind turbine-driven DFIG," in Proc. International Middle East Power Systems Conference (MEPCON), Cairo, Egypt, 2016, pp. 597–603, doi: 10.1109/MEPCON.2016.7836953.

[73] S. S. Rauth, D. Kastha, and P. Bajpai, "A modified MRAS-based sensorless control of DFIG in wind energy conversion system," in Proc. IEEE IAS Global Conference on Emerging Technologies (GlobConET), Arad, Romania, 2022, pp. 863–868, doi: 10.1109/GlobConET53749.2022.9872427.

[74] Y. Sumanth, G. Sambasiva Rao, and K. N. Dharani, "Optimized FOPID controller for doubly-fed induction generator-based wind turbine using root tree optimization algorithm," International Journal of Renewable Energy Research, vol. 15, no. 2, pp. 373–388, 2025, doi: 10.20508/ijrer.v15i2.14783.g9061.

[75] A. Mohammed, E. Ahmed, N. Tamou, and H. C., "Comparative analysis of ADRC and PI controllers used in wind turbine system driving a DFIG," International Journal of Renewable Energy Research, vol. 7, no. 4, pp. 1816–1824, 2017.

[76] R. R. Hete, T. Shrivastava, R. Dash et al., "Design and development of PI controller for DFIG grid integration using neural tuning method ensembled with dense plexus terminals," Scientific Reports, vol. 14, p. 7916, 2024, doi: 10.1038/s41598-024-56904-7.

[77] L. Rayane and S. Lekhchine, "Fuzzy logic controller-based power control of DFIG based on wind energy systems," International Journal of Smart Grid, vol. 8, no. 1, pp. 74–80, 2024, doi: 10.20508/ijsmartgrid.v8i1.334.g346.

[78] H. Benbouhenni, N. Bizon, and M. Yessef et al., "Experimental analysis of genetic algorithm-enhanced PI controller for power optimization in multi-rotor variable-speed wind turbine systems," Scientific Reports, vol. 15, p. 1407, 2025, doi: 10.1038/s41598-024-81281-6.

[79] B. Ibrahim et al., "Optimal power control based-metaheuristic algorithm based variable speed wind energy system of DFIG," in Proc. International Conference on Smart Grid (icSmartGrid), Paris, France, 2023, pp. 1–7, doi: 10.1109/icSmartGrid58556.2023.10170786.

[80] P. Singh, K. Arora, U. C. Rathore, E. Yang, G. P. Joshi, and K. C. Son, "Performance evaluation of grid-connected DFIG-based WECS with battery energy storage system under wind alterations using FOPID controller for RSC," Mathematics, vol. 11, pp. 2100, 2023, doi: 10.3390/math11092100.

[81] H. Bekhada et al., "Comparative study of PI, RST, sliding mode and fuzzy supervisory controllers for DFIG-based wind energy conversion system," International Journal of Renewable Energy Research, vol. 5, no. 4, pp. 1174–1185, 2015.

[82] Z. Zeghdi, L. Barazane, Y. Bekakra, and A. Larabi, "Improved backstepping control of a DFIG-based wind energy conversion system using ant lion optimizer algorithm," Periodica Polytechnica Electrical Engineering and Computer Science, vol. 66, no. 1, pp. 43–59, 2022, doi: 10.3311/PPee.18716.

[83] F. Mohammed, E. Ahmed, N. Mohamed, and N. Tamou, "Control and optimization of a wind energy conversion system based on doubly-fed induction generator using nonlinear control strategies," International Journal of Renewable Energy Research, vol. 9, no. 1, pp. 44–55, 2019, doi: 10.20508/ijrer.v9i1.8812.g7619.

[84] S. K. Adapa et al., "Whale optimization-based PI control for DFIG wind energy systems with modular multilevel grid-side converter," International Journal of Smart Grid, vol. 9, no. 2, pp. 94–104, 2025, doi: 10.20508/ijsmartgrid.v9i2.413.g384.

[85] S. Feleke et al., "Damping of frequency and power system oscillations with DFIG wind turbine and DE optimization," Sustainability, vol. 15, p. 4751, 2023, doi: 10.3390/su15064751.

[86] B. Youcef and B. A. Djilani, "Comparison study between SVM and PWM inverter in sliding mode control of active and reactive power control of a DFIG for variable speed wind energy," International Journal of Renewable Energy Research, vol. 2, no. 3, pp. 471–476, 2012.

[87] C. Dardabi, S. C. Álvarez, and A. Djebli, "An artificial neural network-based direct power control approach for doubly fed induction generators in wind power systems," Energies, vol. 18, p. 1989, 2025, doi: 10.3390/en18081989.

[88] M. Mihir and M. Bhinal, "Modified rotor flux estimated direct torque control for double fed induction generator," International Journal of Renewable Energy Research, vol. 12, no. 1, pp. 124–133, 2022, doi: 10.20508/ijrer.v12i1.12615.g8380.

[89] F. Mazouz, B. Sebti, and I. Chihi, "DPC-SVM of DFIG using fuzzy second-order sliding mode approach," International Journal of Smart Grid, vol. 5, no. 4, pp. 174–182, 2021, doi: 10.20508/ijsmartgrid.v5i4.219.g178.

[90] M. T. Seyed, A. P. Mohammad, and R. Z. Mohammad, "Comparison between different DPC methods applied to DFIG wind turbines," International Journal of Renewable Energy Research, vol. 3, no. 2, pp. 446–452, 2013.

[91] G. Reza, M. Ali, and S. A. Davari, "A new control algorithm method based on DPC to improve power quality of DFIG in unbalanced grid voltage conditions," International Journal of Renewable Energy Research, vol. 8, no. 4, pp. 2228–2238, 2018.

[92] M. M. Alhato and S. Bouallègue, “Direct power control optimization for doubly fed induction generator based wind turbine systems,” Mathematical and Computational Applications, vol. 24, p. 77, 2019, doi: 10.3390/mca24030077.

[93] W. Ayrira, M. Ourahoua, B. El Hassouni, and A. Haddi, “Direct torque control improvement of a variable speed DFIG based on a fuzzy inference system,” Mathematics and Computers in Simulation, vol. 167, pp. 308–324, 2020, doi: 10.1016/j.matcom.2018.05.014.

[94] S. Younes et al., “New intelligent direct power control of DFIG-based wind conversion system by using machine learning under variations of all operating and compensation modes,” Energy Reports, vol. 7, pp. 6394–6412, 2021, doi: 10.1016/j.egyr.2021.09.075.

[95] S. Mahfoud, A. Derouich, N. El Ouanjli, M. El Mahfoud, and M. Taoussi, “A new strategy-based PID controller optimized by genetic algorithm for DTC of the doubly fed induction motor,” Systems, vol. 9, p. 37, 2021, doi: 10.3390/systems9020037.

[96] S. Mahfoud, A. Derouich, A. Iqbal, and N. El Ouanjli, “Ant-colony optimization direct torque control for a doubly fed induction motor: An experimental validation,” Energy Reports, vol. 8, pp. 81–98, 2022, doi: 10.1016/j.egyr.2021.11.239.

[97] Y. Quan, L. Hang, Y. He, and Y. Zhang, “Multi-resonant-based sliding mode control of DFIG-based wind system under unbalanced and harmonic network conditions,” Applied Sciences, vol. 9, p. 1124, 2019, doi: 10.3390/app9061124.

[98] N. A. Yusoff, A. M. Razali, K. A. Karim, T. Sutikno, and A. Jidin, “A concept of virtual-flux direct power control of three-phase AC-DC converter,” International Journal of Power Electronics and Drive Systems, vol. 8, no. 4, pp. 1776–1784, 2017, doi: 10.11591/ijpeds.v8i4.pp1776-1784.